

# VYSOKÉ UČENÍ TECHNICKÉ V BRNĚ

BRNO UNIVERSITY OF TECHNOLOGY

FAKULTA INFORMAČNÍCH TECHNOLOGIÍ  
ÚSTAV INTELIGENTNÍCH SYSTÉMŮ

FACULTY OF INFORMATION TECHNOLOGY  
DEPARTMENT OF INTELLIGENT SYSTEMS

## LIVENESS DETECTION ON FINGERS USING VEIN PATTERN

DIPLOMOVÁ PRÁCE

MASTER'S THESIS

AUTOR PRÁCE

AUTHOR

Bc. TOMÁŠ DOHNÁLEK

BRNO 2015



**VYSOKÉ UČENÍ TECHNICKÉ V BRNĚ**  
BRNO UNIVERSITY OF TECHNOLOGY



**FAKULTA INFORMAČNÍCH TECHNOLOGIÍ**  
**ÚSTAV INTELIGENTNÍCH SYSTÉMŮ**

FACULTY OF INFORMATION TECHNOLOGY  
DEPARTMENT OF INTELLIGENT SYSTEMS

# LIVENESS DETECTION ON FINGERS USING VEIN PATTERN

DETEKCE ŽIVOSTI PRSTŮ NA ZÁKLADĚ ŽIL

**DIPLOMOVÁ PRÁCE**

MASTER'S THESIS

**AUTOR PRÁCE**

AUTHOR

**Bc. TOMÁŠ DOHNÁLEK**

**VEDOUcí PRÁCE**

SUPERVISOR

**doc. Ing. MARTIN DRAHANSKÝ, Ph.D.**

BRNO 2015

## Abstrakt

Tato práce se zabývá rozšířením snímače otisků prstů Touchless Biometric Systems 3D-Enroll o jednotku detekce živosti prstu na základě žil. Bylo navrženo a zkonstruováno hardwarové řešení s využitím infračervených diod. Navržené softwarové řešení pracuje ve dvou různých režimech: detekce živosti na základě texturních příznaků a verifikace uživatelů na základě porovnávání žilních vzorů. Datový soubor obsahující přes 1 100 snímků jak živých prstů tak jejich falsifikátů vznikl jako součást této práce a výkonnost obou zmíněných režimů byla vyhodnocena na tomto datovém souboru. Na závěr byly navrženy materiály vhodné k výrobě falsifikátů otisků prstů umožňující oklamání detekce živosti pomocí žilních vzorů.

## Abstract

This work presents liveness detection extension of the Touchless Biometric Systems 3D-Enroll fingerprint sensor which is based on finger vein pattern. Hardware solution was designed and realized using infrared diodes. Designed software system operates in two different modes: liveness detection based on texture features and user verification using finger vein matching. A dataset containing more than 1,100 images of both real fingers and their falsifications was gathered. Performance of both proposed modes was evaluated using mentioned dataset and suitable materials, that can fool the liveness detection module, were highlighted.

## Klíčová slova

biometrie, detekce živosti, otisky prstů, žíly prstů, spoofing, TBS, absorpce světla hemoglobinem

## Keywords

biometrics, liveness detection, fingerprint, finger vein, spoofing, TBS, haemoglobin light absorption

## Citace

Tomáš Dohnálek: Liveness Detection on Fingers Using Vein Pattern, diplomová práce, Brno, FIT VUT v Brně, 2015

# Liveness Detection on Fingers Using Vein Pattern

## Prohlášení

Prohlašuji, že jsem tuto diplomovou práci vypracoval samostatně pod vedením doc. Ing. Dipl.-Ing. Martina Drahanského, Ph.D. Další informace mi poskytl Bc. Adam Trhoň. Uvedl jsem všechny literární prameny a publikace, ze kterých jsem čerpal.

.....  
Tomáš Dohnálek  
26. května 2015

## Poděkování

Na tomto místě bych rád poděkoval doc. Ing. Dipl.-Ing. Martinu Drahanskému, Ph.D. za možnost pracovat na této práci a za vstřícný přístup. Rád bych také poděkoval všem dobrovolníkům, kteří se nechali nasnímat, a na závěr Ivce, která mě vždy podporovala a motivovala.

© Tomáš Dohnálek, 2015.

*Tato práce vznikla jako školní dílo na Vysokém učení technickém v Brně, Fakultě informačních technologií. Práce je chráněna autorským zákonem a její užití bez udělení oprávnění autorem je nezákonné, s výjimkou zákonem definovaných případů.*

# Contents

<b>1</b>	<b>Introduction</b>	<b>3</b>
<b>2</b>	<b>Biometrics Overview</b>	<b>4</b>
2.1	Fundamentals . . . . .	4
2.2	Evaluating Performance of Biometric Systems . . . . .	5
2.3	Advanced Topics . . . . .	6
<b>3</b>	<b>Fingerprint Recognition</b>	<b>7</b>
3.1	Biological Background . . . . .	7
3.2	Sensing . . . . .	8
3.3	Feature Extraction . . . . .	10
3.4	Matching . . . . .	11
3.5	Summary . . . . .	11
<b>4</b>	<b>Liveness Detection on Fingers</b>	<b>13</b>
4.1	Vulnerabilities of Biometric Systems . . . . .	13
4.2	Liveness Detection . . . . .	14
4.3	Summary . . . . .	17
<b>5</b>	<b>Finger Vein Recognition</b>	<b>18</b>
5.1	Biological Background . . . . .	18
5.2	Sensing . . . . .	19
5.3	Pre-processing . . . . .	21
5.4	Feature Extraction . . . . .	25
5.5	Classification and Matching . . . . .	29
<b>6</b>	<b>Proposed Liveness Detection System Based on Finger Vein Pattern</b>	<b>31</b>
6.1	Image Acquisition . . . . .	31
6.2	Pre-processing . . . . .	34
6.3	Quality Assessment . . . . .	37
6.4	Feature Extraction . . . . .	38
6.5	Classification and Matching . . . . .	39
<b>7</b>	<b>Implementation</b>	<b>40</b>
7.1	Sensing Subsystem . . . . .	40
7.2	Evaluation Subsystem . . . . .	40
7.3	Quality Annotator . . . . .	41

<b>8 Evaluation</b>	<b>42</b>
8.1 Dataset Description . . . . .	42
8.2 Quality Assessment . . . . .	43
8.3 Liveness Detection . . . . .	43
8.4 Finger Vein Recognition . . . . .	45
8.5 Concluding Remarks . . . . .	45
<b>9 Conclusion</b>	<b>47</b>

# Chapter 1

## Introduction

The number of developed biometric systems and even used biometric characteristics is increasing. The most known and widely acceptable is fingerprint authentication, which is nowadays often used in attendance systems and also has been integrated to laptops and mobile systems.

Despite the fact, that fingerprint recognition algorithms for extraction and comparison are very sophisticated and show high performance, security risks still occur. Fingerprints can be easily reproduced from a latent fingerprint of unaware users, and then used to gain an unauthorized access to a system. It has been shown, that most commercial fingerprint systems can be fooled by using an artificially created fingerprints, and therefore liveness detection is being integrated.

Liveness detection is a countermeasure against attempts to fool the biometric system with a fake fingerprint. An example of liveness detection method is detection of finger veins. Among main advantages of using finger vein pattern for biometric purpose is that blood vessels are an internal characteristic of a person and an image of it cannot be acquired as easily as fingerprints.

The goal of this thesis is to design and implement a liveness detection prototype system using finger vein pattern and extend an existing fingerprint sensor Touchless Biometric Systems 3D-Enroll. The proposed solution is inexpensive and requires only additional infrared Light-Emitting Diodes (LEDs). The system can work in two different modes: liveness detection and finger vein recognition. In the first mentioned, a classification task, decision between live and non-live has to be made. On the other hand, in finger vein recognition mode, veins are extracted and compared with appropriate user template. Together fingerprint and finger vein recognition can create a powerful multimodal biometric system. Experimental results demonstrate potential of both proposed approaches using gathered dataset containing more than 1,100 images of both live fingers and non-live falsifications.

Fundamental biometric terminology is presented in [Chapter 2](#). Fingerprint recognition is described in [Chapter 3](#), various liveness detection approaches are studied in [Chapter 4](#) and methods of acquiring finger vein images and its further processing steps are discussed in [Chapter 5](#). The design of the proposed liveness detection system is presented in [Chapter 6](#) and its implementation in [Chapter 7](#). Finally, the system performance is evaluated in [Chapter 8](#).

## Chapter 2

# Biometrics Overview

This chapter introduces biometric related terminology necessary for comprehension of the following chapters. Rather than giving exhaustive explanation, only terms, which are used in this work, are explained with possibility for the reader to follow references to learn more about particular terms.

### 2.1 Fundamentals

**Biometric system** A system for automated recognition of individuals based on their behavioral or physiological characteristics is called the biometric system [1].

**Biometric characteristic** Biometric characteristics (or traits [2]) can be divided into two categories: physiological and behavioral. The former category includes the physical properties of a body such as fingerprints, vein patterns, iris, etc. The latter one refers to the behavioral processes created by the human body, such as voice, walking or keystroke dynamics [1].

**Biometric feature** Biometric data acquired by a biometric sensor are processed in order to get salient discriminatory features, which represent underlying biometric trait [2].

**Template** A template is a compact representation of a biometric source [3] (a set of biometric features [1]) usually encrypted and stored in a biometric system for comparison with biometric features.

**Identification** A biometric system can work either in identification or in verification mode [2]. In the former mode, the system task is to recognize person's identity by comparing captured biometric data with all templates stored in a database. There is no need for the person to claim his identity. If a match in the database is found, the person gains identity of the user with matching template. This type of recognition is also called *one-to-many* and is generally more demanding, because the system needs to compare biometric features with all templates in the database (several people might have similar templates and correct distinguishing decision has to be made), but is considered to be more comfortable for users.



**Verification** On the other hand, in verification mode [2], an individual claims to be a user of a system and the system will perform a *one-to-one* comparison with the particular user's template. According to similarity rate with this template, the individual gains the identity of the user or not.

## 2.2 Evaluating Performance of Biometric Systems

To be able to compare a quality of biometric systems, a performance of biometric system must be defined. To express the similarity of two biometric features a *similarity score* [2] is defined. The score is called *genuine* if two samples from the same individual are compared. On the other hand, if two samples from different users are compared, the score is called *impostor*.

If the genuine score decreases below threshold  $\eta$ , the user is not recognized by the system. Such situation is denoted as a False Reject (FR). If the impostor score exceeds threshold  $\eta$ , then the impostor is incorrectly recognized as a user of the system and such situation is called False Accept (FA).

**False Accept Rate** False Accept Rate (FAR) is defined as a fraction of impostor scores exceeding the threshold  $\eta$  [2].

**False Reject Rate** False Reject Rate (FRR) is defined as a fraction of genuine scores falling below the threshold  $\eta$  [2].

**Failure to Acquire** Failure to Acquire (FTA) rate is defined as a fraction of attempts a sensor fails to acquire a sample although it was presented to it [2]. This situations often occur due to inability of a sensor to acquire a biometric signal of a sufficient quality. FTA can be used as a measure of a quality of biometric sensors [4].

**Failure to Enroll** Failure to Enroll (FTE) rate is defined as a proportion of users that cannot be enrolled by a biometric system [2]. This include users which are not able to interact with a sensor properly.

**False Match Rate** False Match Rate (FMR) is calculated similarly to FAR, but in the calculation there are excluded unsuccessful attempts which failed before actual comparison (caused by FTE or FTE).

**False Non-Match Rate** False Non-Match Rate (FNMR) is computed similarly to FRR, but there are not included unsuccessful attempts caused by FTE or FTE.

**Detection Error Tradeoff curve** The knowledge of only the FAR or the FRR of the system is worthless, since the threshold  $\eta$  can be set to very high values and therefore almost all impostors will be rejected by the system. On the other hand, very few genuine users will be accepted. That is why, when mentioning performance of a system, both FAR and FRR must be presented.

We can see that FRR and FAR are both dependent on threshold  $\eta$ . FAR and FRR can be visualized in a single graph denoted as a Detection Error Tradeoff (DET) curve [2], where horizontal axis is FAR and vertical axis is FRR for various values of  $\eta$ . If both

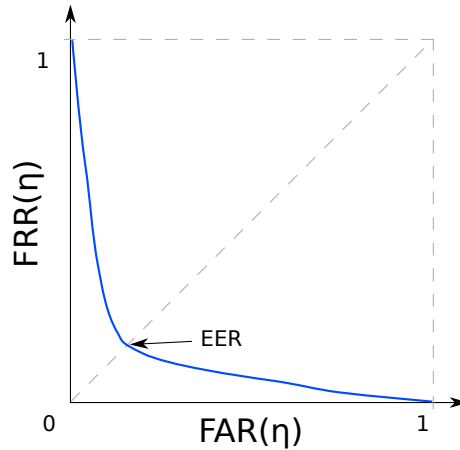


Figure 2.1: Example ROC curve dependent on threshold  $\eta$  together with highlighted EER point.

axes are displayed in linear, logarithmic, or semi-logarithmic scale, the graph can be called Receiver Operating Characteristic (ROC) curve.

**Equal Error Rate** The point in DET curve where FAR and FRR are equal is denoted as a Equal Error Rate (EER) and can be used as a single-value measure of biometric system performance. Example of ROC curve and EER point is visualized in [Figure 2.1](#).

## 2.3 Advanced Topics

**Multimodal biometric systems** Nowadays, most biometric system is unimodal – they measure single biometric feature (e.g. only fingerprint or only face). On the contrary, multimodal biometric systems [5] measure two or more features of a single person and therefore they are considered to be more reliable. Due to combination of more characteristics, it is also more difficult for impostor to spoof the system. There are different fusion levels, but generally speaking, earlier the fusion of biometric features is performed, the more effective system is considered. Nevertheless, not all features are compatible for fusion at level of extracted features. More often approach is integration in similarity score levels.

**Liveness Detection** The capability of a biometric system to detect whether a provided biometric sample is alive or not is denoted as a liveness detection [6]. Its main purpose is to detect spoofing and therefore it is often called spoof detection or anti-spoofing measure.

## Chapter 3

# Fingerprint Recognition

The first scientific paper concerning fingerprints and its biological background was published by Nehemiah Grew in 1684 [4]. Since then, many other scientists started their own research about fingerprints and fingerprint recognition. Based on the empirical observations, fingerprints are considered unique for each individual [2], and they can be easily classified into nine different categories. Soon, the fingerprint identification was adopted and systematically used in forensics. Collected databases of fingerprints started to be so large that manual comparison was non-maintainable and automatic methods for comparison had to be invented.

Nowadays, fingerprints are one of the most wide-spread and well-known biometric characteristic, due to its long history, which concluded in the public acceptance of this method. Not only forensic but also civilian application are successfully developed. Due to the high intraclass variability of fingerprints and decreasing prices of both sensing and evaluating devices the fingerprint recognition is being adopted by more solutions such as Automated Teller Machines (ATMs), personal computer logons and physical access control [2].

This chapter presents background to understand fingerprints from biological point of view. Next, various fingerprint sensors are described and finally, feature extraction and matching is outlined.

### 3.1 Biological Background

Skin consists of three layers: epidermis, dermis and hypodermis [7, 3]. The epidermis, the most outer non-vascular skin layer, is moulded on the papillary layer. Its thickness varies – on palms of hands and soles of feet the epidermis is thicker, harder, and has hornier texture than on the rest of the body.

Dermis (or corium) is the vascular layer and, same as epidermis, it is thicker on palms and soles of feet. Hypodermis is the thickest inner part of skin. There is stored variable amount of fat, therefore the hypodermis participates in thermoregulation and also large blood vessels can be found there.

Fingerprints are the patterns formed by epidermal ridges on fingers. Shapes of epidermal ridges are determined by the transition from dermis to epidermis in the papillary layer as displayed in [Figure 3.1](#). Ridges start to establish from the 10<sup>th</sup> week of the pregnancy and develop until the 16<sup>th</sup> week [8]. It was empirically observed that since the 16<sup>th</sup> week, the ridges become permanent, even though they can be damaged, altered or destroyed completely [9].

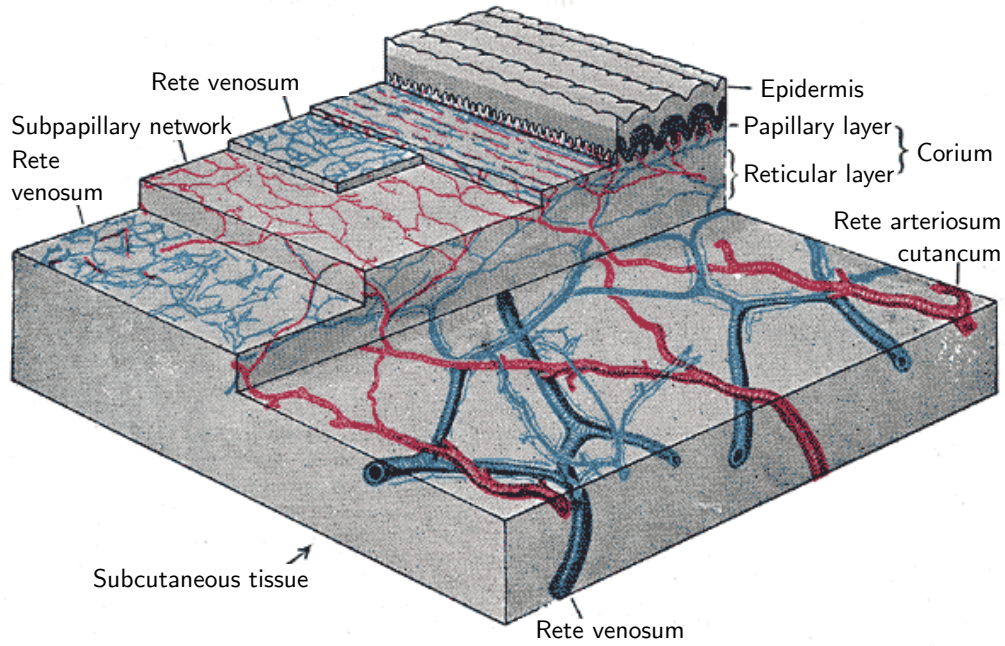


Figure 3.1: Skin layers. Source: [7].

## 3.2 Sensing

There was no need for a special hardware for acquiring fingerprint images in the past, because fingerprints were kept on dactyloscopic cards using black ink or other dye. These images then could be digitized via a scanner; this method is called off-line sensing [2].

For live-scan sensing, there is no need for the ink – a person just needs to place its finger near the electronic fingerprint scanner. The first generation of on-line sensors were based on optical technology [6], but others such as solid-state or ultrasound were invented.

### 3.2.1 Technologies

There are various approaches how an image can be captured and as a consequence how a user has to interact with a sensor.

**Touch** Most of the sensors are based on a touch technology. The user has to place a finger on the sensor and keep it still for a moment until an image is taken [6]. This technique requires almost no training and user guidance. On the contrary, touch based sensors can become dirty and have to be cleaned in order to preserve good quality of taken image. Sweat and dirt caused by previous users might be repulsive for someone, and can be a cause of diseases transmission. Security reasons also occur – latent fingerprints can be used for reactivation attacks [10]. Last but not least, the sensor size must be large enough to capture even wide fingertips and that causes higher price of such device.

The touch based devices are also denoted as area, or placement sensors [11].

**Sweep** Next generation of sensors is based on sweep technology. In comparison to touch sensors, sweep ones are wide as a finger but only a few pixels high. As a consequence,

on sweep based sensors there remain no latent fingerprints, and it has partly self-cleaning property. Nevertheless some drawbacks remain: there is still need for user to touch the sensor with all its disadvantages, and even new drawbacks occur. Learning of sensor handling is more demanding. User might need few tries before suitable fingerprint image could be acquired. Also there are higher demands on image processing hardware, since the whole fingerprint image must be reconstructed from several partial images. [6]

**Touchless** Touchless based sensors [11] are the latest generation of fingerprint sensor technology. The finger is presented to the sensor from various distances (starting from a few centimeters, up to a few meters<sup>1</sup>) and the fingerprint is captured from distance (usually using camera). Touchless technology solves not only the hygienic and security (latent fingerprints) issues from foregoing generations [12], but also addresses disadvantage of nonuniform finger pressure, present in touch and sweep based sensors. It also lowers the need for maintenance of such system. On the other hand, it opens new ways for spoofing, it might be hard for user to position the finger, and since there is no physical support for the finger. Also, the optical (or other technology) system must be adapted to acquire image of trembling fingers.

### 3.2.2 Optical sensors

In the touch variation of optical sensing, the finger touches a side of a glass as depicted in Figure 3.2a. The epidermal ridges are in contact with the surface, but valleys (spaces between ridges) remain at a distance from the surface [2]. The finger is then illuminated by visible light and the light is reflected by valleys and randomly absorbed by epidermal ridges. The reflection is captured by the camera and due to the lack of reflection of ridges, it is possible to distinguish between ridges and valleys on acquired image.

Described mechanism was improved during time, and for example electro-optical sensors emerged. They do not illuminate a finger, but the finger touches a light-emitting polymer. According to the pressure (ridges touch the surface, but valleys do not) corresponding amount of light is generated by the polymer. The incident light is again captured by Charge Coupled Device (CCD), Complementary Metal Oxide Semiconductor (CMOS), or a photodiode array. [6]

Not only reflective method, where light is reflected from the finger, but also transmission methods exist [11]. The red light with wavelength around 660 nm is emitted and due to skin tissue's high transmittance ratio, the light penetrates through the finger and it is recorded by the camera.

Optical methods are best suitable for touch and touchless based approaches.

### 3.2.3 Solid-state sensors

Solid-state sensors, also denoted as silicon sensors [2], are two-dimensional arrays of tiny sensors, each representing single pixel. The user then touches the surface of the sensor and according to used type of the sensor (including capacitive, thermal, or piezoelectric) the physical information is converted to an electronic signal and further to a digital image.

---

<sup>1</sup>Fingerprint sensor AIRprint is designed for a long range sensing up to two meters: <http://www.idairco.com/products/>

**Capacitive** In case of the capacitive technology, the array elements are micro-capacitor plates [6], which are more frequent than epidermis ridges, see Figure 3.2b. Since ridges directly touch the surface of a sensor, the change of capacitance is higher than in case of the valleys, which are further. These capacitance differences are used to acquire digital image of the fingerprint [6].

**Thermal** Thermal sensors consist of pyro-electric cells [4] which are sensitive to temperature differences. Skin (the ridges) has usually higher temperature than the air in the valleys and therefore an image of the fingerprint can be reconstructed. Since the air in valleys might get warm enough very quickly, this approach is used mainly with sweep technology [6].

**Piezoelectric** Sensitive sensors produce electric signal, when stress is applied to them. The quantity of generated current is depended on pressure, and as a consequence there is produced more current in areas where ridges touch the sensor than in valley areas. [13]

### 3.2.4 Ultrasound sensors

Ultrasound sensors are based on capturing echoed signals, which were originally sent to the fingertip, see Figure 3.2c. The received signal is then used to compute the distance and subsequent fingerprint pattern. The sensor is composed of a transmitter, which produces short pulses (from few kilohertz up to several gigahertz in order to acquire high resolution [6]), and a receiver, which detects echoed signals from fingerprint surface [13].

This technology is not mature enough – a few seconds are required to acquire an image and the price of these sensors remain higher than previously described sensors.

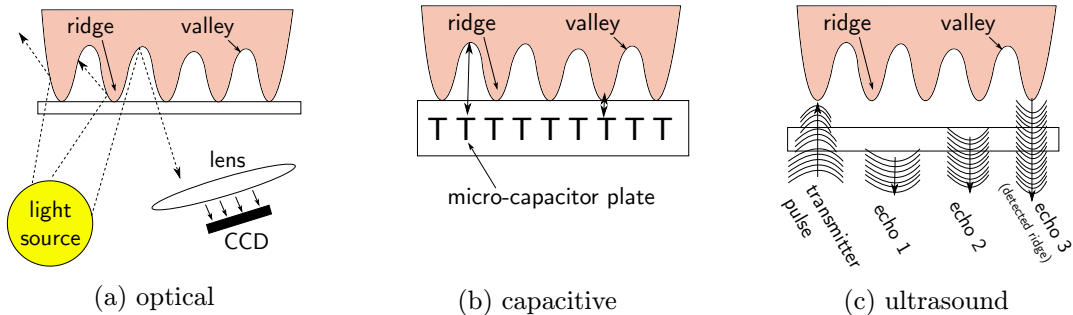


Figure 3.2: Three types of fingerprint sensors: (a) *optical* – reflective method with glass and external light source (inspired by [4]); (b) *capacitive* – representative of solid-state family (inspired by [13]); (c) *ultrasound* (inspired by [13]).

## 3.3 Feature Extraction

Due to all kinds of distortions and noise of acquired images from sensors, the comparison of fingerprint image and stored template cannot be computed directly by cross-correlation or Euclidean distance. On the contrary, unique features are extracted, because it has been proven to be more robust solution [14].

There are three commonly used features – Directional Field (DF), Singularity Points (SPs) and minutiae. The DF is a coerce description of a fingerprint and it is defined [14]

as a local orientation of the ridge-valley structures. DF can be derived from gradients by performing average operations on them.

SP are significant points in a fingerprint image, where the ridge lines assume distinctive shapes [2]. There are two types of SP – deltas and cores. The topmost point of the innermost curving ridge [14] is called the *core* and a center of triangular region where three different direction flows meet is the *delta*. Each fingerprint contains at most two deltas and two cores [14]. Another usage of SP, except utilization as a feature, is to use these significant points to align two compared images. There are several approaches how to obtain singularity points for example, DF can be used [14].

The most commonly used features in automatized physical access control systems are called minutiae. The minutiae extraction converts grayscale fingerprint image to several points in image such as bifurcations and end-points. The first step of the extraction process is image enhancement used to suppress the noise in the image and to enhance the ridge-valley structures [14]. After that, a binarization is performed, which converts grayscale image into binary one. Usually a single global threshold value for binarization is not sufficient (due to various gray level characteristics in image, caused, for example, by nonuniform pressure of finger on sensor), and dynamic thresholding has to be applied. Once the binary image is obtained, ridges should be visually separable, but the ridges have various thickness and therefore thinning is applied resulting into so called skeleton of the image [14]. From the skeleton image, it is easy to decide where minutiae are located, but many false minutiae appear. These are caused by high noise in original image and therefore post-processing algorithms are performed to suppress fake minutiae.

### 3.4 Matching

Once the feature vector is extracted from an input image, it can be compared with stored template and similarity score is determined. In case of minutiae feature vector, this stage is called minutiae matching [14] or point pattern matching problem [2].

Combination of local and global minutiae matching is usually used for determining the rotation and translation of input image due to stored template, where local matching examines local structures, which are invariant with respect to global transformation (translation, rotation, etc.). In this step, list of possibly corresponding minutiae is obtained and the size of the list is the first indication of degree of similarity of two fingerprints.

In global matching phase, the global translation and rotation of acquired fingerprint image is found and list of possibly matching minutia is reduced and based on the size and distance, the matching score is determined.

It must be mentioned, that other non-minutiae matching methods (such as texture based and others) are developed [2], because extracting minutiae from highly noised fingerprint images is very difficult and also the operations are very time consuming.

### 3.5 Summary

Fingerprints are pioneer of biometric characteristics in automatic recognition. They has been widely accepted and has a good reputation due to its uniqueness [2] – even identical twins have different epidermal ridges. The character of the ridges-valley structure stays stable through the whole life [4, 8], which makes fingerprints suitable for long-term recognition. Last but not least the performance of fingerprint recognition is very high – for example,

commercial Touchless Biometric Systems (TBS)<sup>2</sup> claims to have fingerprint system with FRR less than 0.5% at FAR equal 0.001% in verification mode.

Fingerprints are physiological characteristic which means they can be damaged. User may (un)intentionally harm his finger and make the recognition impossible [9]. There are also security issues. Most users are not observant to fact, that they leave their latent fingerprints on many places – glasses, doors, etc. Such latent fingerprints can be used to create artificial fingertip to fool the sensor and to obtain unauthorized access to a system.

Therefore, there is no wonder that many researchers put a lot of effort in spoofing fingerprint systems and, at the same time, developing anti-spoofing mechanisms, which will be described in next chapter.

---

<sup>2</sup>[http://www.tbs-biometrics.com/fileadmin/tbs-media/products/3D-Enroll/en\\_productsheet\\_3d-enroll.pdf](http://www.tbs-biometrics.com/fileadmin/tbs-media/products/3D-Enroll/en_productsheet_3d-enroll.pdf)



## Chapter 4

# Liveness Detection on Fingers

Alert Wehde's attempt to compromise the fingerprint based recognition systems is dated to 1920s [2]. He took a photo of an enhanced latent fingerprint and etched the fingerprint onto a copper plate, which could be used to leave counterfeit latent prints. Many researches [2, 15, 6] showed, that modern materials – with more similar characteristics to human skin than a copper – can be used to create artificial fingertips for fooling live scan sensors. Fingerprint recognition systems become more frequent, and therefore attacks on them have to be explored (only four days after Samsung Galaxy S5 with swipe based fingerprint sensor was released, the first successful spoofing attack is reported<sup>1</sup>), and countermeasures against these attacks have to be developed.

In this chapter, vulnerabilities of the fingerprint biometric systems will be described with focus on attacks on sensor level. After that, a survey of liveness detection methods on fingers will be presented.

### 4.1 Vulnerabilities of Biometric Systems

FAR measures the ability of a system to stand up against so called *zero-effort attacks*, when attacker simply presents his own biometric characteristic to a sensor and tries to be recognized as another person. This is an example of the most elementary attack, but there exist many other types of attacks on all subsystems of the biometric system; for full list see [2, 15]. In this work, only presentation – on sensor level – vulnerabilities will be considered, because other vulnerabilities are common to all software and can be resolved by traditional cryptographic tools or by having vulnerable subsystems at a secure location, or under a supervision [15].

To the attack category at sensor level belongs placing fake finger on the sensor surface and replay attack (resubmitting previously stored biometric sample [15]). A spoofing is an attack, when a person is pretending to be anyone else and presenting the system a fake biometric sample. In this chapter, there will be put an emphasize on fingerprint systems spoofing.

Intruder can fool the system with *registered finger* – this includes obscure situations, when intruder gives the legitimate user an anesthetics and then he uses the sleeping user's finger or he can even separate the finger from the user's body to obtain an unauthorized

---

<sup>1</sup><http://www.computerworld.com/article/2476130/cybercrime-hacking/researchers-spoof-fingerprint--bypass-samsung-galaxy-s5-security--access-paypal.html>

access. [6]. Protections against these situations have been explored, but they usually worsen the user experience.

Another type of attack is using *unregistered finger* in order to obtain unauthorized access, but this threat is measured by FAR.

Using an *artificial finger* in order to fool the system is the most common discussed attack [6, 15, 2]. In case of spoofing fingerprint systems, the finger can be made as a whole from gelatin, silicone, play-doh, clay, latex [6], or can be just a thin layer which is be glued to intruder’s finger and presented to the sensor.

There are also other types of attacks, such as using a generic clone of a finger or reactivation of residual fingerprint on the sensor [10].

## 4.2 Liveness Detection

The capability of a biometric system to detect whether the provided biometric sample is alive or not is denoted as *liveness detection* [6] and its main purpose is to detect spoofing. Liveness detection methods can be divided into three categories [2].

1. Using only data collected for biometric purposes.
2. Using further processed information collected in order to generate discriminating features or by sensing the biometric sample in time.
3. Using additional hardware.

There are two ways how to determine whether a presented biometric sample is alive or not – liveness detection focuses on unique properties of human body parts and non-liveness detection focuses on typical properties of materials used to fool the system. A survey of commonly used liveness detection properties of human fingers follows.

**Perspiration** One of several liveness detection methods without any additional hardware is using natural perspiration behavior of skin [15]. However, a sensor with a camera producing fingerprint images with very high resolution is needed. There are about 600 sweat glands per square inch in human skin [6, 15], which diffuse sweat to the surface of the skin through pores. The pore-to-pore distance on fingertip is approximately 0.5 mm and the position of pores is stable through time.

When a capacitive sensor is used to obtain a fingerprint image, the capacitance of the ridges and valleys (air) is measured and the sweat on fingertip ridge causes higher capacitance value measured by the sensor. The longer the finger is put on a touch based sensor, the more is moist and therefore the more darker image becomes.

There are two basic approaches how to use this information: static and dynamic. In the static approach, only single image of fingerprint is used and the decision about liveness is based on fact that the fingerprint will look “patchy” due to the high number of pores. On the other hand, in the dynamic approach at least two images should be captured with some time difference (in original paper [16] is stated 5 seconds) and the darkness level is compared.

**Multi-spectral analysis** Skin and underlying layers of a finger interact in different manners with light in various wavelength spectrum – they have unique optical characteristics. For example, water absorption coefficient starts to dramatically raise from 900 nm [15], other components of living tissue have their own specifics.

Example of usage of this information was utilized by Lumidigm company<sup>2</sup>, which developed a new approach for not only liveness detection, but this characteristic can be also used as individual biometric feature. The principle lies in measuring the amount of reflected light of different wavelengths from finger skin and sublayers.

**Pulse based on oxygen level** Pulse oximetry is a non-invasive approach to measure the oxygen-level in blood [3]. These systems are often used in medicine, but they seem to be convenient also for liveness detection. Oxygen saturation ratio is used to decide whether a presented sample is alive or artificial. It is computed as a ratio of concentration of oxygenated haemoglobin ( $HbO_2$ ) and sum of concentrations of oxygenated ( $HbO_2$ ) and deoxygenated ( $Hb$ ) haemoglobin in systematic arterial blood.

Due to spectral absorbance character of both  $HbO_2$  and  $Hb$ , depicted in Figure 4.1, two different sets of LEDs are used to capture both types of haemoglobin – LEDs in wavelength of 660 nm to capture  $Hb$  and 920 nm [3] (or 940 nm [15]) to capture  $HbO_2$ . There can be used either transmission method, when LEDs are located from one side of a finger and a camera on the opposite, or reflection method, when LEDs are located on the same side of the finger as the camera. With the pulse, the intensity of transmitted (or reflected) light in camera changes, and the pulse frequency itself can be detected and used for liveness detection. Unfortunately, pulse oximetry does not work reliably with smokers, because smoking raises level of carboxyhaemoglobin ( $COHb$ ) in blood, which cannot be distinguished from  $HbO_2$  [3]. Also, the measured characteristics are influenced by dyes and skin pigments and therefore can vary from person to person [15].

**Temperature** The temperature of human epidermis of the finger is in range of approximately 25-37°C [15] and this information can be used to detect a live sample. The intraclass variability of such a feature is quite high, due to various weather and health conditions, and therefore the system must be very moderate with values of stated temperature ranges. It has been proved that if intruder glues a thin layer with artificial fingerprint on his own fingertip, the temperature difference will be no more than 2°C. Therefore, using temperature as a liveness detection is not considered to be reliable [4, 6, 15].

**Pressure** Skin has usually reddish color, but when pressure is applied, the skin color turns whitish. Such a skin property can be used in touch based sensors. It has been shown that light in spectral range 640-770 nm [15], used to reflect from fingertip, does not show any substantial difference between pressed and not pressed state of fingertip. On the other hand, light in blue and green spectrum (from 400 nm to 600 nm) shows variance.

**Electrical** Liveness detection based on electrical properties is a family of methods, including conductivity and Relative Dielectric Constant (RDC) [15, 6].

The conductivity of skin is based on humidity, which varies from individual to individual [15]. There are people with dry fingers and, on the other hand, some people have

---

<sup>2</sup>[http://www.biometrics.org/bc2005/Presentations/Conference/Wednesday%20September%2021/Wed\\_Ballroom%20B/Rowe\\_Multispectral\\_BC05.pdf](http://www.biometrics.org/bc2005/Presentations/Conference/Wednesday%20September%2021/Wed_Ballroom%20B/Rowe_Multispectral_BC05.pdf)

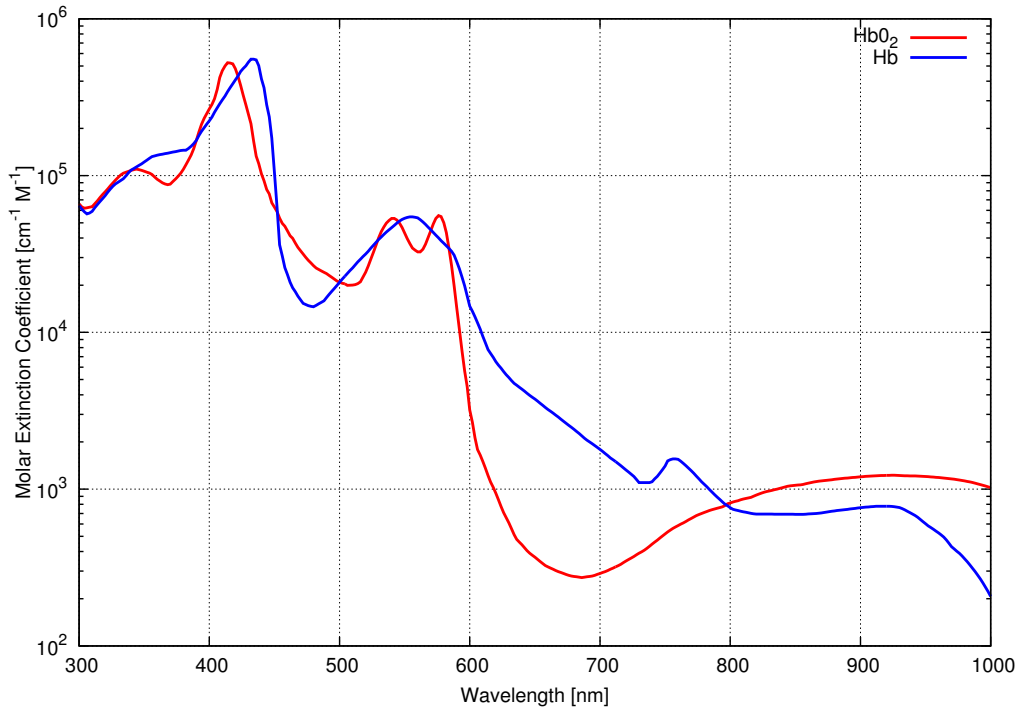


Figure 4.1: Absorption properties of oxygenated ( $HbO_2$ ) and deoxygenated ( $Hb$ ) haemoglobin in relation with wavelength. Based on [17].

constantly sweaty hands. The level of conductivity is also dependent on environmental conditions, which result in a wide range of allowed resistance level. As a consequence, intruder can then easily fool the system as described in [6].

RDC expresses the degree to which a material resists the flow of electric charge [6]. The value of RDC is the discriminating factor between a real and an artificial finger, but similarly to the conductivity, the different humidity of fingers makes it easy to fool the system.

**Multimodal approach** Using additional biometric modalities increases the difficulty to attack the biometric system at the sensor-level [3]. It is more demanding for the attacker, because he needs to elicit additional biometric data from the valid user and create an additional artificial sample, which has to be accepted by the attacked biometric system.

Except fingerprints, several other finger characteristics can be measured, such as finger veins patterns, geometry of the finger, finger nail bed, finger knuckle [3].

Using the same physical part of body for multimodal biometric system, which can capture all biometric characteristics concurrently or with a very small delay, is more comfortable for the user. On the other hand, it makes it easier for the impostor to acquire the user's characteristic.

**Other** There are many other approaches for liveness detection: a method based on odor analysis [11], different methods for pulse detection [18], bio-impedance [4], ultrasonic detector [15], and challenge-response mechanism could be used, but description of all these is beyond this thesis' scope.

There are also probably commercial solutions of liveness detection, but they usually stay hidden, because companies are not willing to discuss their solutions. This approach, called *security through obscurity*, makes it initially more difficult for the impostor to attack the system. On the other hand, the hidden method can have issues, which could be revealed by discussion. But if the solution was made public, the attacker could benefit from such information.

### 4.3 Summary

Liveness detection is an important part of every secure biometric system. Few non-invasive methods for liveness detection were presented in previous paragraphs. Every approach has its weaknesses and strengths. Probably all of them are possible to fool, but with every such countermeasure, it demands higher amount of effort, more knowledge about the systems and more money to get through.

Liveness detection on fingers using blood vessel patterns – a multibiometric system – will be presented in next chapters.

## Chapter 5

# Finger Vein Recognition

Joseph Rice, an employee of Kodak, proposed an idea of biometric recognition based on infrared image of hand in 1983 [19]. The idea has evolved, and nowadays, imaging veins of a single finger is promising biometric approach achieving high recognition performance.

The biological background of the mentioned method will be presented in this chapter. Next, the processing pipeline, various extracted feature and related algorithms will be described.

### 5.1 Biological Background

The cardiovascular systems can be found in humans and animals [3] and its fundamental function is to maintain the homeostasis – a constant set of conditions within cells. There are two circles in the cardiovascular system: pulmonary and systemic. The first mentioned loops from the heart to the lungs, where oxygen-depleted blood is re-oxygenized. In the latter one, the oxygen-saturated blood is carried from the heart by a network of blood vessels to all parts of the body and backwards to the heart [3].

There are three major types of blood vessels: arteries, capillaries and veins. The arteries carry oxygen-saturated blood from the heart. The capillaries allow substances and liquids to exchange between the blood and tissue, and finally, veins carry the blood from capillaries back to the heart. The character of these vessels differs – while the arterial walls are very thick and strong (to be able to handle high pressure blood), the vein walls are thinner, more flexible, and the diameter of veins is larger. The capillaries are the smallest of vessels with inner diameter around  $8\ \mu\text{m}$  [3]. The diameter of both veins and arteries decreases proportionally to the distance from the heart. The outermost blood vessels are located directly below epidermis, as can be seen in [Figure 3.1](#), but the main trunks are located deeper in hypodermis. Generally, veins are located closer to the skin in comparison to arteries. Example of blood vessels of the back of a hand can be seen in [Figure 5.1](#).

Blood consists of fluid plasma, in which three kinds of blood corpuscles are suspended [7, 3] – erythrocytes (99%), leucocytes (less than 1%) and thrombocytes (less than 1%). Erythrocytes consist of iron-containing protein *haemoglobin*, which can bind oxygen. Due to presence of oxygenated haemoglobin ( $\text{HbO}_2$ ) in oxygen saturated blood, carried by arteries, the blood has a bright red color and oxygen-depleted blood in veins has a dark red or violet color due to the presence of deoxygenated haemoglobin (*Hb*).

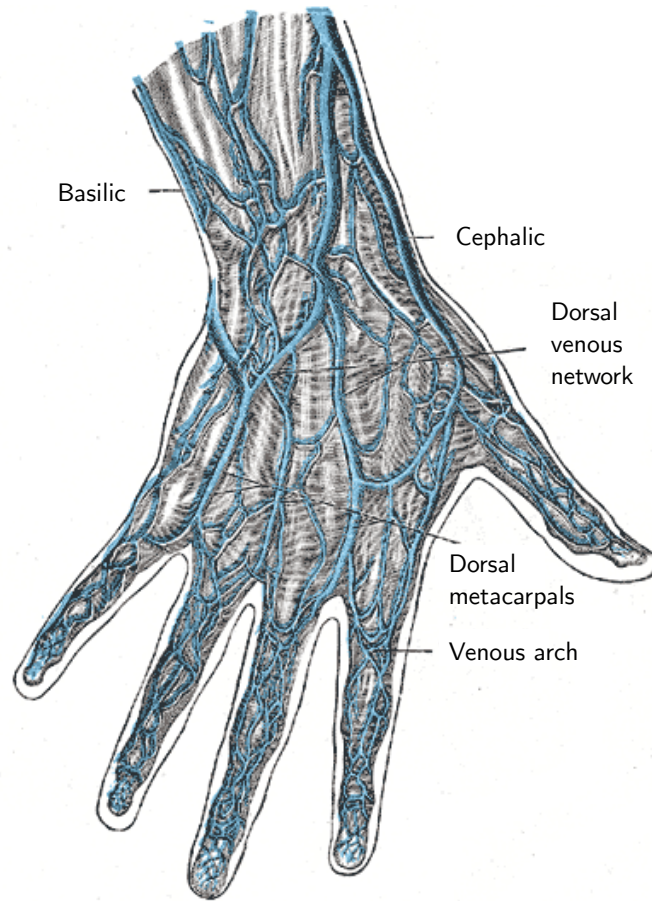


Figure 5.1: The veins on the dorsum of the hand. Source: [7].

## 5.2 Sensing

There are several ways [3] how to acquire an image of human blood vessels, such as using X-ray, magnetic resonance imaging, ultrasound, far-infrared light, near-infrared light or thermal approach [20]. The near-infrared light approach is used most often in biometrics due its tradeoff between cost, power supplement requirements, size of the sensor and quality of resulting image.

The two types of haemoglobins ( $Hb$ ,  $HbO_2$ ) have different absorption spectra as can be seen in Figure 4.1. Experiments have proved that the permeability of human tissue is high for electromagnetic radiation in range from 600 nm to 1,300 nm [3, 21], this range is often called *optical window*. Especially in the range between 750-950 nm [3], the radiation can penetrate deep enough into the skin to reach the superficial arteries and veins, and as a consequence it is absorbed in blood vessels, due to higher absorption coefficient blood. This effect can be captured by a camera – spots on the image where blood vessels are located are darker.

Even though described method can capture not only veins, but also arteries, this method for capturing blood vessels will be further denoted as a vein characteristic.

There are two main methods of acquiring an image of blood vessels of a finger with Near Infrared (NIR) approach – reflection and transmission.

### 5.2.1 Reflection Method

Even though the NIR reflection illumination setup is usually used for acquiring palm, palm dorsal and wrist vein images, it is possible to use it also for finger vein acquisition [3, 22, 23]. The finger is illuminated by NIR light, and the partially reflected radiation is captured by a CCD camera, which is located on the same side of the finger as the light emitter. Because veins are closer to the skin than arteries, veins are usually captured on resulting image. Simplified schema of a finger vein sensor using reflection method can be seen in Figure 5.2a.

The main advantages of this approach are the sensor size, compactness and possibility to easily extend existing (fingerprint) systems with finger vein recognition system.

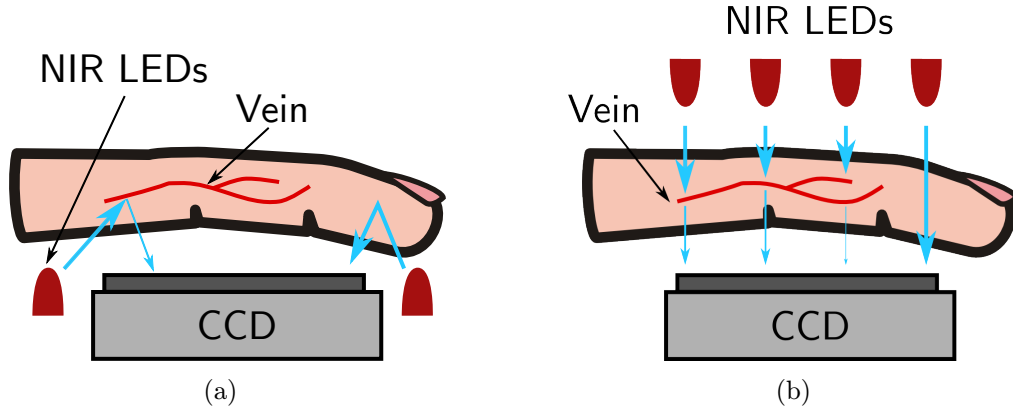


Figure 5.2: Two main approaches for acquiring finger vein pattern using NIR light: (a) reflection method; (b) transmission method.

### 5.2.2 Transmission Method

The transmission method is usually used only in finger vein recognition, because fingers are generally thin enough to allow the light to pass through the tissue. The NIR light emitter is in such case located on the opposite side of the finger than the camera. Although the transmission method is leading in finger vein sensing, it must be mentioned, that the device itself is usually larger than the one using reflection method. On the other hand, the quality of resulting image is more high-contrasted in comparison to reflection approach [23]. Simplified schema of a finger vein sensor using reflection method can be seen in Figure 5.2b.

### 5.2.3 Wavelength of Light Emitters

The range, where the permeability of human tissue is high, is very wide – from 600 nm to 1,300 nm [3]. The absorbency of haemoglobin also differs. Until today it has not been proven, to the best of our knowledge, which wavelength is generally the best suitable for transmission and reflection method.

Nevertheless, Fuksis (2010) [20] was trying to answer this question for palm vein sensing, but the answer is not general. Yang and Shi (2014) [24] describe a finger vein sensor using 760 nm LEDs with declaration, that this is the optimal light source wavelength to capture veins. Despite the fact, several systems with various wavelengths of the light emitter are developed as can be seen in survey in Table 5.1. From this table, it is obvious, that the most promising interval starts at 750 nm and ends at 900 nm. The number of LEDs used



Table 5.1: Survey of developed finger vein sensors for research purposes.

Device	Method	Wavelength [nm]	Details
[24, 25]	transmission	760	additional visible light from sides
[26]	transmission	790	
[27]	transmission	808	3× LED
[28]	transmission	850	
[29]	transmission	850	
[30]	transmission	850	6× LED
[31]	transmission	850	6× LED
[32]	transmission	850	8× SFH4550
[33]	transmission	850	
[22]	reflection	850	
[34]	transmission	870	40× LED
[35]	transmission	890	
[23]	transmission	N/A	NIR LEDs are from side of a finger

to illuminate the finger also varies from 3 to 40, but it should be mentioned, that most of the research papers do not state the number or even type of used LEDs.

### 5.3 Pre-processing

In this section, pre-processing algorithms used for finger vein recognition and liveness detection will be described. First, the segmentation approach will be presented, after that various approaches to normalize the finger and eliminate finger posture changes will be defined. Next, survey of contrast enhancement methods will be presented, and finally automatic quality estimation algorithms of finger vein images will be outlined.

#### 5.3.1 Segmentation

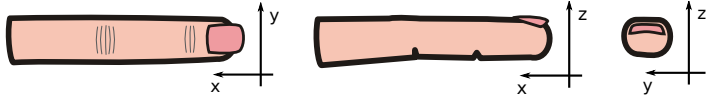



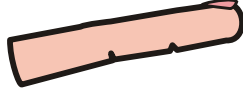
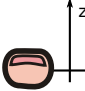
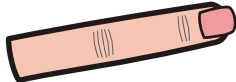
To one of many segmentation algorithms belongs Watershed method [36]. The gray level function of an image is perceived as an altitude function and the images becomes a topographical surface. Some predefined local minima are then defined to be a source of a water. The water floods uniformly higher lying areas, while the water level is uniform over the whole surface and it increases with uniform speed. When water from two different water sources should met, a dam is built to prevent merging. After the whole surface is flooded, only dams are visible and they define contours and separate segments. [36]

This approach can be successfully used to segment image if precise position of distinguished classes are known.

#### 5.3.2 Finger Posture Changes

Conventional finger vein systems use touch based sensors, and quite often the finger posture changes are ignored, with minimum impact on system performance. However, when a touchless sensor is utilized, the finger posture change correction cannot be omitted, since the difference in two images of the same finger can be great. In [37], six basic kinds of finger posture changes are defined and they are displayed and described in Table 5.2.

Table 5.2: Defined coordinate system and six finger posture changes. Based on [37].

Type	Name	
1	shift along x-axis	
2	rotation around x-axis	
3	shift along y-axis	
4	rotation around y-axis	
5	shift along z-axis	
6	rotation around z-axis	

These changes can be categorized into two categories: 2D and 3D changes. Types 1, 3 and 6 are 2D changes and are usually dealt with in comparison algorithm. On the other hand Types 2, 4 and 5 are called 3D changes and need to be treated separately and the possible solution using single camera is presented in [38] and following [37]. The main idea is to represent 3D finger model as a set of *oval* slices (e. g. slices of a cylinder), which is transformed into flatten surface.

### 5.3.3 Interphalangeal Joint

The phalangeal joints of a finger are constituted by several components including synovial fluid [25], which density is much lower than density of bones. Therefore, when using transmission method to acquire a finger vein image, a brighter region can be seen in the acquired image, which corresponds to the interphalangeal joint. This region can be substituted by a single line with a pixel width [25]. The knowledge of the position of this line could be utilized to estimate rotation, translation and even scale changes of the finger posture.

In [25], the Type 6 change is ignored and sum of all gray level values for each column (perpendicular to the length of the finger) is computed as in Equation (5.1) and the maximum row-sum in Equation (5.2) approximately denotes the position of the interphalangeal joint.

$$\phi(x) = \sum_{y=1}^{y_{max}} f(x, y) \quad (5.1)$$

$$r_k = \operatorname{argmax}_{x \in \{1, \dots, x_{max}\}} (\phi(x)) \quad (5.2)$$

### 5.3.4 Contrast Enhancement

Since finger vein images are usually quite noisy and unevenly illuminated, it is crucial to enhance the image to be able to distinguish between veins and the tissue. To achieve good contrast and even illumination, the iterative control of lighting is often used. However, this method requires more complex hardware and additional software control. If no such improvement is used, it is necessary to perform pre-processing before the actual feature extraction. [3]

In [3], a comprehensive survey of commonly used methods for finger vein contrast enhancement is presented. Spatio-Temporal Retinex-like Envelope with Stochastic Sampling (STRESS), Partitioned Iterated Function System (PIFS), Contrast Limited Adaptive Histogram Equalization (CLAHE), Linear Unsharp Masking and Wang methods are compared using several metrics including time complexity analysis. Although the STRESS algorithm is usually perceived the best for image enhancement, it also significantly enhances the noise presented in image. According to [3], the level of negative influence is too high, and the author recommends using CLAHE method. The result of both image contrast enhancement algorithms is shown in Figure 5.3.

The CLAHE [39] is an extension of Adaptive Histogram Equalization (AHE). The image is divided into several tiles and for each tile a histogram normalization is performed. After that an interpolation scheme is used to avoid the visibility of different tile boundaries. In CLAHE extension, a constant clip limit  $c$  is defined, which limits the histogram bin to contain the  $c$  pixels at most. If more pixels should be inserted into the bin, they are redistributed over the whole histogram instead.

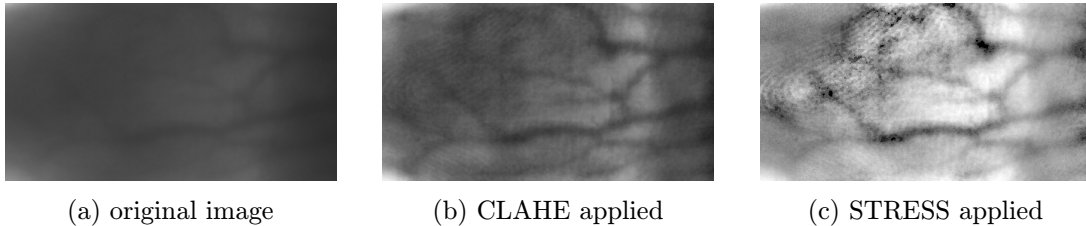


Figure 5.3: Comparison of contrast enhancement methods.

### 5.3.5 Quality Assessment

Due to the high noise presented in finger vein images, it is useful to evaluate images and assign it with quality scores reflecting the vein visibility. A low quality references, created by the system for comparison, could cause a poor performance of the systems. [3]

The reasons for poor quality are caused mainly due to inappropriate user behavior. The user could accidentally move the finger during sensing, or incorrectly place the finger on the sensor.

In [3, 40, 41] a Gray Level Co-occurrence Matrix (GLCM) and Haralick features were successfully utilized in order to estimate the quality. GLCM is a texture analysis tool [40] and is defined as “a two dimensional histogram of gray levels for a pair of pixels, which are separated by a fixed relationship” [42]. The fixed relationship is described by a displacement vector  $v$ , consisted of a distance  $d$  and a direction  $\theta$ . GLCM is a square matrix and its size is derived from image depth and is equal to number of different possible colors in the

image. Each element  $(i, j)$  of GLCM matrix is calculated using [Equation \(5.3\)](#).

$$P(i, j, d, \theta) = |\{[(x_1, y_1), (x_2, y_2)] \mid f(x_1, y_1) = i \wedge f(x_2, y_2) = j \wedge \text{dis}((x_1, y_2), (x_2, y_2)) = d \wedge \angle((x_1, y_2), (x_2, y_2)) = \theta\}|, \quad (5.3)$$

where  $\text{dis}$  is distance metric,  $\angle$  is the angle between pixels  $(x_1, y_2), (x_2, y_2)$ , and  $f$  is a pixel intensity function [\[40\]](#). Example of GLCM matrices are displayed in [Figure 5.4](#).

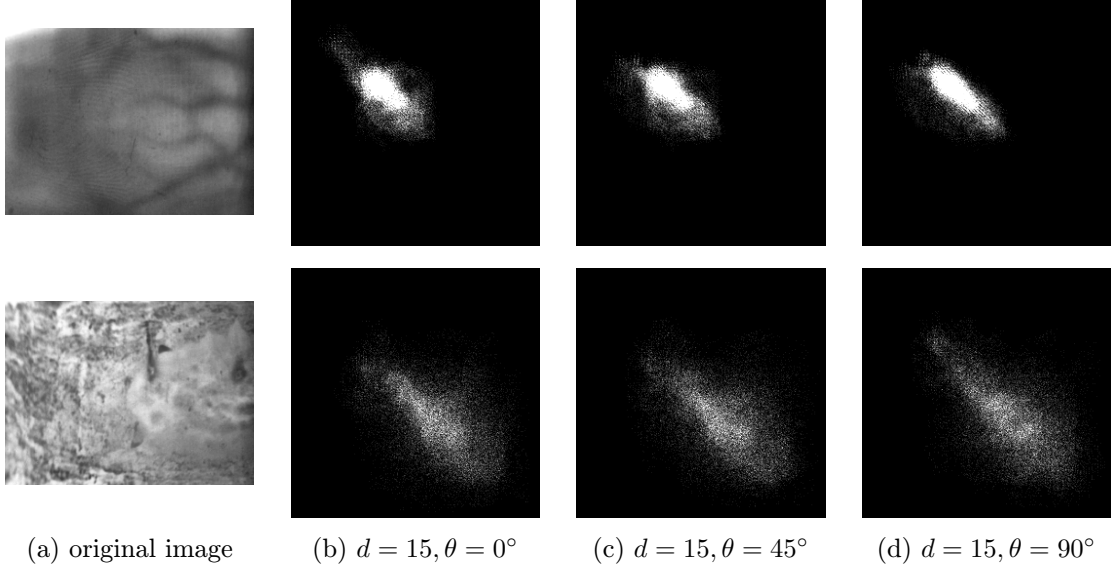


Figure 5.4: Example of GLCM matrices for image of real finger veins (1<sup>th</sup> row) and carrot (2<sup>nd</sup> row) and various displacement vectors.

In case of image, which does not have the same size, it is useful to work with normalized GLCM matrices computed using [Equation \(5.4\)](#).

$$P_{norm}(i, j, d, \theta) = \frac{P(i, j, d, \theta)}{x_{max} \cdot y_{max}}, \quad (5.4)$$

where  $x_{max}$  ( $y_{max}$ ) is the number of columns (rows) of the examined image.

Based on the GLCM matrix, we can compute 14 Haralick features, which are a different way how to describe a texture of the image. The features include:

$$Energy = \sum_{i,j} P(i, j, d, \theta)^2 \quad (5.5)$$

$$Contrast = \sum_{i,j} |i - j|^2 \cdot P(i, j, d, \theta) \quad (5.6)$$

$$Homogeneity = \sum_{i,j} \frac{P(i, j, d, \theta)}{1 + |i - j|} \quad (5.7)$$

$$Entropy = - \sum_{i,j} P(i, j, d, \theta) \cdot \log(P(i, j, d, \theta)) \quad (5.8)$$

These features can be used not only to estimate the quality of the image, but also as a features used for classification.

## 5.4 Feature Extraction

In this section, various features, which could be extracted from finger vein images will be described.

### 5.4.1 Local Binary Patterns

Local Binary Patterns (LBP) is a method for extracting textural features of a grayscale image. The original LBP [43] uses  $3 \times 3$  non-parametric operator for labeling each pixel  $(x_c, y_c)$  by thresholding the eight-neighborhood with the gray level of the center pixel  $(x_c, y_c)$  and summing thresholded values weighted by powers of two [44]. The resulting LBP value is for each pixel  $(x_c, y_c)$  defined in Equation (5.9).

$$LBP(x_c, y_c) = \sum_{n=0}^7 s(f_n - f_c) \cdot 2^n \quad (5.9)$$

$$s(x) = \begin{cases} 1 & \text{if } x \geq 0 \\ 0 & \text{if } x < 0 \end{cases}$$

where  $f_c$  represents a gray level value of the center pixel  $(x_c, y_c)$  and  $f_n$  is a gray level value of corresponding neighbor pixel. Example of computation of LBP value of a single pixel can be seen in Figure 5.5.

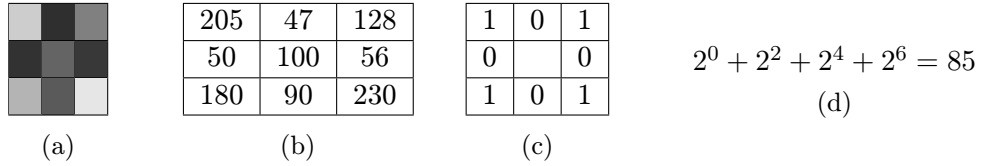


Figure 5.5: Computation of LBP value of a single pixel: (a) grayscale image; (b) gray level values of the image; (c) thresholded neighborhood; (d) LBP value of the center pixel.

The operator can be extended to use neighborhoods with different radius and various neighbor counts. Such LBP variations are denoted as  $LBP_{P,R}$ , where  $P$  corresponds to neighbor count and  $R$  to radius. There are more variants of LBP [44], which can be rotation invariant or have some additional properties. In extension Local Binary Patterns Histogram (LBPH), the LBP image is divided into  $n$  regions  $R_1, \dots, R_n$  from which histograms are extracted and then concatenated into a single histogram. [45, 46]

LBP and its variations are widely and successfully used in vein recognition [47, 43, 48] due to high performance even when the image is irregularly shaded or there are saturated regions.

### 5.4.2 Repeated Line Tracking

The Repeated Line Tracking [49] method extracts finger vein pattern even from a noised and irregularly shaded image. Even though the resulting vein pattern can be promising, the time required for processing is quite high in comparison to other described methods. The method is based on tracking dark lines starting at various pixel positions. The dark line is followed until it is not detectable anymore, and then a new line from different pixel is started. Tracking is recorded to a separate matrix called locus space, which shows

probability of vein presence. Although some noise might be recorded as well, statistically it is less emphasized than the veins [49].

The process of vein extraction [49] is divided into five separate steps. In the first step, a starting point  $C = (x_c, y_c)$  is selected using Monte Carlo method, or (as suggested by authors) various heuristics for choosing the point can be utilized in order to decrease the time demands of the algorithm. The global locus space  $T_r$  is incremented at the position  $C$ . After that, a random moving-direction  $D_{lr}, D_{ud}$  attribute to determine the orientation of vein is chosen according to Equation (5.10).

$$D_{lr} = \begin{cases} (1, 0) & \text{if } rnd < 0.5 \\ (-1, 0) & \text{otherwise} \end{cases} \quad D_{ud} = \begin{cases} (0, 1) & \text{if } rnd < 0.5 \\ (0, -1) & \text{otherwise} \end{cases} \quad (5.10)$$

where  $rnd$  is a random number from interval  $[0, 1)$  generated using uniform distribution. This prevents the algorithm from following lines with excessive curvature.

In the second step, the actual dark line is tracked. Another local locus space  $T_c$  is used just for this step to mark already visited pixels in order to avoid trapping in local maximum. Based on the current point  $C$ , the local locus space and the preset direction  $D$  a set of neighbor pixels  $N_r$  is selected as a potential following of the dark line according to Equation (5.11).

$$N_r(C) = \begin{cases} N_3(D_{lr}, C) & \text{if } rnd < p_{lr} \\ N_3(D_{up}, C) & \text{if } p_{lr} \leq rnd < p_{lr} + p_{ud} \\ N_8(C) & \text{otherwise} \end{cases} \quad (5.11)$$

$$N_3(D, C) = \{(C_x + D_x, C_y + D_y), \\ (C_x + D_x - D_y, C_y + D_y - D_x), \\ (C_x + D_x + D_y, C_y + D_y + D_x)\}, \quad (5.12)$$

where  $p_{lr}$  ( $p_{ud}$ ) is a preset probability of selecting neighbor pixels in horizontal (vertical) direction.  $N_8(C)$  is the set of eight neighbor pixels next to  $C$  and  $N_3(D, C)$  is the set of three neighbor pixels of  $C$  in orientation of moving direction, mathematically expressed in Equation (5.12).

A set of candidate pixels forming the dark line, denoted as  $N_c$  and expressed in Equation (5.13), contains all pixels from  $N_r$ , which were not visited so far.

$$N_c = N_r \cap \bar{T}_c, \quad (5.13)$$

where  $\bar{T}_c$  is a binary complement of a local locus space  $T_c$ .

The crucial step is to choose the pixel from  $N_c$ , which is the following of dark line. The choice is determined according to gray level values of cross-sectional profiles in direction of all candidates in  $N_c$ . The best candidate  $B$  is computed using Equation (5.14) and Equation (5.15).

$$E((x_i, y_i), (x_c, y_c)) = f(x_c, +r \cos \theta - \frac{W}{2} \sin \theta, y_c, +r \sin \theta + \frac{W}{2} \cos \theta) \\ + f(x_c, +r \cos \theta + \frac{W}{2} \sin \theta, y_c, +r \sin \theta - \frac{W}{2} \cos \theta) \\ - 2 \cdot f(x_c, +r \cos \theta, y_c, +r \sin \theta) \quad (5.14)$$

$$B(N_c, C) = \operatorname{argmax}_{\forall (x_i, y_i) \in N_c} E((x_i, y_i), C) \quad (5.15)$$

$$V_l(N_c, C) = \max_{\forall (x_i, y_i) \in N_c} E((x_i, y_i), C), \quad (5.16)$$

where  $W$  is the width of cross-sectional profile,  $r$  is distance between  $(x_c, y_c)$  and cross-section.  $\theta$  is the angle between line segments  $(x_c, y_c) - (x_c + 1, y_c)$  and  $(x_c, y_c) - (x_i, y_i)$ . If  $V_l > 0$  then update starting point  $C = B(N_c, C)$  and repeat the second step except initializing the local locus matrix. If  $V_l \leq 0$ , then proceed to step three. Visual example of computation the candidate  $B$  from given set  $N_c$  can be seen in [Figure 5.6](#).

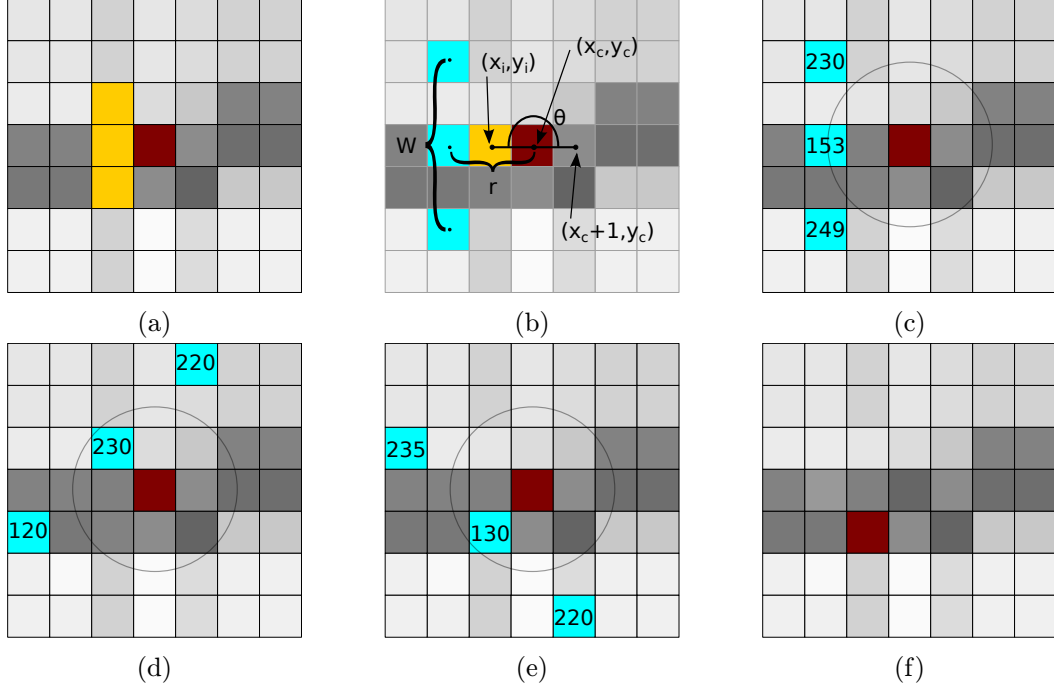


Figure 5.6: Example of calculation of second step of Repeated Line Tracking feature extraction method. (a) Consider starting point  $\blacksquare (x_c, y_c)$  and  $\blacksquare N_c = N_r = N_3((-1, 0), x_c, y_c)$ . (b) Consider  $W = 4$  and  $r = 2$ .  $(x_i, y_i)$  is the first examined candidate in direction  $(-1, 0) \in N_c$ . The three points used in [Equation \(5.14\)](#) are colored with  $\blacksquare$ . (c)  $E((-1, 0), (x_c, y_c)) = 230 + 249 - 2 \cdot 153 = 173$ . (d)  $E((-1, 1), (x_c, y_c)) = 220 + 120 - 2 \cdot 230 = -120$ . (e)  $E((-1, -1), (x_c, y_c)) = 235 + 220 - 2 \cdot 130 = 195$ . (f) Maximum was gained in (e), so in the next iteration,  $\blacksquare (x_c - 1, y_c - 1)$  will be the new starting point.

In the third step, the values of each element  $(x, y)$  of global locus space  $T_r$  is incremented  $\forall (x, y) \in T_c$ .

The fourth step is iteration from step one to step three  $N$  times. In the last step, the veins are extracted from locus space. The value  $T_r(x, y)$  indicates the probability of being a vein for each pixel  $(x, y)$ . However, only larger chains of high values should be considered as veins, since smaller chains are probably noise.

It should be mentioned, that there are a few variables ( $W$ ,  $r$ ,  $p_{lr}$ ,  $p_{ud}$ , and  $N$ ) in the algorithm and their choice greatly influences the performance.

### 5.4.3 Maximum Curvature

Maximum Curvature [50] is another method for extracting finger veins from an image. It is claimed to be resistant to various vein widths and its brightness. The algorithm has become a benchmark for the newly developed finger vein extraction and comparison methods [51, 34, 32].

The extraction can be divided into three separated steps [50]. In the first step, the centers of veins are extracted using cross-sectional profiles. Consider an image and function  $f(x, y)$ , which gives the gray level value at pixel  $(x, y)$  of the image. A profile  $P_f(z)$  is a cross-sectional profile acquired from  $f(x, y)$  at any direction and position, where  $z$  is a position in a profile. The curvature  $\kappa$  of a such a profile [50] can be calculated as in Equation (5.17).

$$\kappa(z) = \frac{P_f(z)''}{[1 + (P_f(z)')^2]^{\frac{3}{2}}} \quad (5.17)$$

All positive local maxima of all concave areas of the profile's curvature are calculated and these points are the center positions of veins. Complete set of these points is denoted as  $I$ , and for each entry a score  $S_{cr}$  determining the probability that the point is a vein center is defined in Equation (5.18). Example of computing the score can be seen in Figure 5.7.

$$\forall z_i \in I : S_{cr}(z_i) = \kappa(z_i) \cdot W_r(z_i), \quad (5.18)$$

where  $W_r$  is the width of the concave positive area of  $\kappa(z)$  around position  $z_i$ .

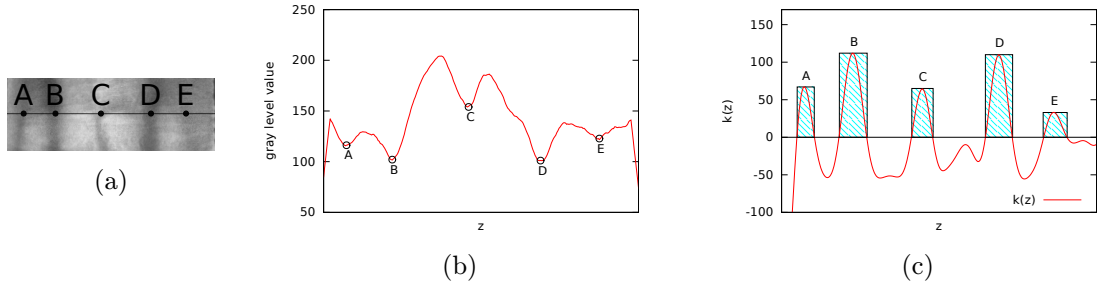


Figure 5.7: Example of calculation veins centers using Maximum Curvature. (a) Original image. Example  $P_f(z)$  is drawn with black line and expected center positions of veins are labeled as A-E. (b) Gray level values of the plane  $P_f(z)$  are visualized with labeled center points. (c) Curvature is calculated and local maxima of concave areas, which are positive, are stated as center points of veins. The area of the blue shaded region is score  $S_{cr}$ , which determines the probability of being a vein center position.

It is reasonable to define  $P_f(z)$  for more than one direction (usually four are used – vertical, horizontal and two oblique) and a total score  $V(x, y)$  is calculated as a sum of these four appropriate scores  $S_{cr}(z_i)$ .

In the second step, the noise reduction is performed using filtering operations. For each pixel, its neighbors in a certain direction are examined and according to Equation (5.19) final score  $G$  is determined.



$$G(x, y) = \max_{(d_x, d_y) \in D} \min \{ \max(V(x + d_x, y + d_y), V(x + 2d_x, y + 2d_y)), \max(V(x - d_x, y - d_y), V(x - 2d_x, y - 2d_y)) \}, \quad (5.19)$$

where  $D = \{(0, 1), (1, 0), (1, 1), (1, -1)\}$ .

In the last step, the function  $G$  is thresholded and binary image of extracted finger veins is received.

## 5.5 Classification and Matching

In this section, algorithms which could be utilized to match templates or classifiers will be briefly outlined.

### 5.5.1 Support Vector Machine

Support Vector Machine (SVM) is a supervised learning technique used for classification and regression analysis [52]. Consider finite set of pairs  $(x_i, y_i)$ , where  $i \in \{1, \dots, l\}$ ,  $x_i \in \mathbb{R}^n$  and  $y_i \in \{1, -1\}$ .  $x_i$  are training vectors, and  $y_i$  is an appropriate class (label) of  $x_i$ . The goal of the linear classifier is to find function that maps  $x \in \mathbb{R}^n$  to a correct  $y$ . In SVM, the training vectors are mapped into a higher dimensional space using a kernel function and then linearly separated using a hyperplane with maximal margin between feature vectors of the two training classes. The closest training vectors from both classes are called support vectors. Sometimes, the training dataset is not perfectly linearly separable, and then the hyperplane is placed to distinguish as much as possible between both classes.

Among the commonly used kernel functions belong linear, polynomial, sigmoid and Radial Basis Function (RBF). [52] It is possible to generalize the SVM to classify into more classes than two, and also to produce a probability distribution over all classes.

### 5.5.2 Iterative Closest Point

Iterative Closest Points (ICP) is a general purpose algorithm for finding a transformation which minimizes a distance between two clouds of points. It is convenient to have the two clouds coarsely aligned (estimate the initial transformation) at the beginning, to avoid trapping in the local minimum, because ICP is a gradient descend method. [53]

Consider cloud point  $P = \{\vec{p}_1, \dots, \vec{p}_{N_p}\}$ , which will be positioned to be in the best alignment with reference cloud  $X = \{\vec{x}_1, \dots, \vec{x}_{N_x}\}$ . Consider Euclidean distance  $d(\vec{a}, \vec{b})$ . The distance between a single point  $\vec{p} \in P$  and the cloud  $X$  is computed as in Equation (5.20).

$$d(\vec{p}, X) = \min_{x \in X} d(\vec{x}, \vec{p}) \quad (5.20)$$

The actual corresponding point to  $\vec{p}$  will be denoted as  $\vec{y}$  and set of all these corresponding points will be denoted as  $Y, Y \subseteq X$ .

$$d(\vec{p}, \vec{y}) = d(\vec{p}, X) \quad (5.21)$$

After that a least squares registration  $Q$  in Equation (5.22) is computed using quaternion math.

$$(\vec{q}, d) = Q(P, Y), \quad (5.22)$$

where  $\vec{q}$  is a desired transformation (rotation and translation) that minimizes the distance between  $P$  and  $Y$  and  $d$  is a mean square point matching error.

Finally, the  $P$  is updated with  $P = \vec{q}(P)$ , where notation  $\vec{q}(P)$  is used to denote the transformation  $\vec{q}$  performed on point cloud  $P$ . These steps are repeated until current mean square error  $d_k$  and mean square error from previous iteration  $d_{k-1}$  satisfy a condition  $d_k - d_{k-1} < \tau$ , where  $\tau$  is a predefined threshold determining the precision. [53]

### 5.5.3 Hamming Distance

Two features vectors of the same length can be compared by Hamming Distance calculated using Equation (5.23).

$$HD = \frac{CodeA \otimes CodeB}{N}, \quad (5.23)$$

where  $CodeA$  is the extracted binary code of feature vector  $A$ ,  $\otimes$  is Boolean exclusive OR and  $N$  is the size of both binary feature vectors. The result value  $HD$  is ranging from 0 to 1 and higher value implies lower similarity. [47]

### 5.5.4 Histogram Comparison

There are several ways how to measure a similarity between two histograms  $A$  and  $B$ , such as using correlation or chi-square methods. The chi-square method is defined as in Equation (5.24) [46].

$$\chi^2(A, B) = \sum_{i=1}^n \frac{(A_i - B_i)^2}{A_i + B_i} \quad (5.24)$$

This method can be successfully utilized to compare two LBPH feature vectors.

## Chapter 6

# Proposed Liveness Detection System Based on Finger Vein Pattern

In this chapter, the proposed liveness detection system is described. The liveness detection can be perceived from a different point of views. The main task is to distinguish presented biometric samples between living and non-living class, and moreover, as mentioned in [Section 4.2](#), the multimodal approach can also be perceived as a liveness detection method. Both of these approaches will be examined and discussed.

The requirements on the proposed system are as follows:

- The system is divided into two separated subsystems – acquisition of images and image processing.
- The first subsystem is built using existing fingerprint sensor.
- The second subsystem must be hardware independent and fully automated – input image is automatically classified as live or non-live without any user input.
- The second subsystem supports a “recognition” mode, which, instead of classification into live or non-live category, verifies registered users.

The design of an architecture of the proposed system is depicted in [Figure 6.1](#). First, the image must be acquired using a separate *image acquisition* subsystem, several images of the same finger can be captured using different settings of a camera to partially deal with various thickness of fingers and finger posture changes. Brief description of used fingerprint sensor and its extension will be described below. After that, in all captured images, the finger is localized and normalized in the *pre-processing* module. From several images captured with various camera settings, the best one with the highest contrast is chosen in the *quality assessment* module. The *feature extraction* module extracts feature vector from the Region of Interest (ROI). Finally, depending on the chosen mode, *classification* or verification (*matching* to appropriate user template) will be performed.

### 6.1 Image Acquisition

First step in liveness detection on fingers is the acquisition of a presented finger. It was chosen to use TBS fingerprint sensor and extend it with liveness detection based on finger

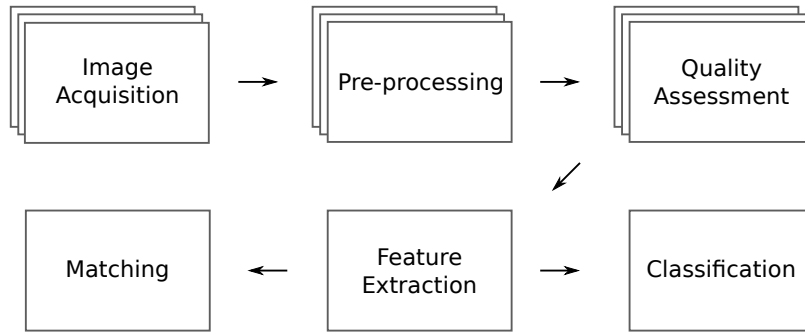


Figure 6.1: Designed architecture of a proposed system.

vein pattern. In this section, the main features of the chosen TBS sensor and its extensions will be described.

### 6.1.1 Touchless Biometric Systems Fingerprint Sensor

Commercial device TBS 3D-Enroll<sup>1</sup> is a three-dimensional touchless sensor for enrollment and generation of fingerprint templates. There are three cameras inside the sensor as can be seen in Figure 6.2 and several LEDs of various colors.

It should be mentioned, that the sensor is designed to acquire only a fingertip and therefore user inserts only this part of the finger into the box. Size of both veins and arteries is decreasing with the distance from heart. For vein recognition, usually the most interesting are parts of finger areas near the middle and proximal phalanges. The blood vessels near distal phalanx are hardly visible, but only image of this finger part is acquirable using this device.

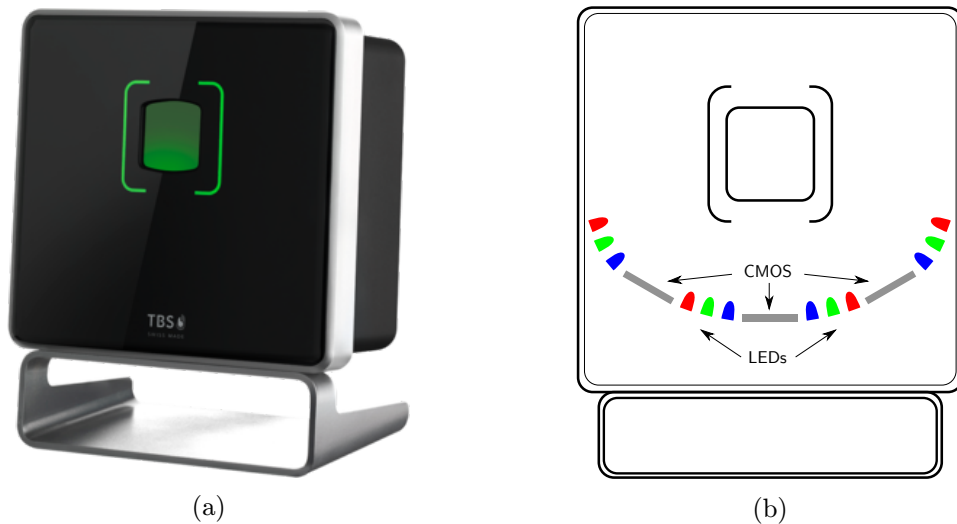


Figure 6.2: TBS 3D-Enroll sensor: (a) photo of the device (Source: Official TBS website); (b) simplified schema.

<sup>1</sup>[http://www.tbs-biometrics.com/fileadmin/tbs-media/products/3D-Enroll/en\\_productsheet\\_3d-enroll.pdf](http://www.tbs-biometrics.com/fileadmin/tbs-media/products/3D-Enroll/en_productsheet_3d-enroll.pdf)

### 6.1.2 Extension of Existing Sensor

Two different methods of sensing were discussed in [Section 5.2](#): reflection and transmission. The main disadvantages of transmission method are the size of the device and that a user has to put his finger into a “black box”. On the other hand, it seems, that the transmission method gives images, where the finger veins are more visible and easily distinguishable in comparison to reflection method. Since all these disadvantages are already present in TBS sensor, the transmission method was chosen in order to obtain a more high-contrast images.

A decision to utilize only the middle camera for this prototype was made, but in future, all three cameras could be used to reconstruct the 3D model of blood vessels of the finger. A board was constructed that five NIR LEDs could be mounted to the top of the fingerprint sensor and the construction allowed effective changing of LEDs and the voltage. The board is powered from the sensor’s main power supply, so no additional power supply is needed. Both sketch and wiring diagram of proposed circuit can be seen in [Figure 6.3](#). LEDs are connected in parallel in order to allow to set different levels of intensity for each LED, because the fingertip thickness and tissue characteristic varies for each individual. Many finger vein solutions [[38](#), [49](#), [23](#)] use automatic brightness control to eliminate such individual variations, thus the system can be extended with this automated approach. This solution was not incorporated in this work, because it increases both hardware and software demands. After several experiments, we decided to give the resistor  $R_1$  higher resistance in comparison to others ( $R_2 = R_3 = R_4 = R_5$ ).

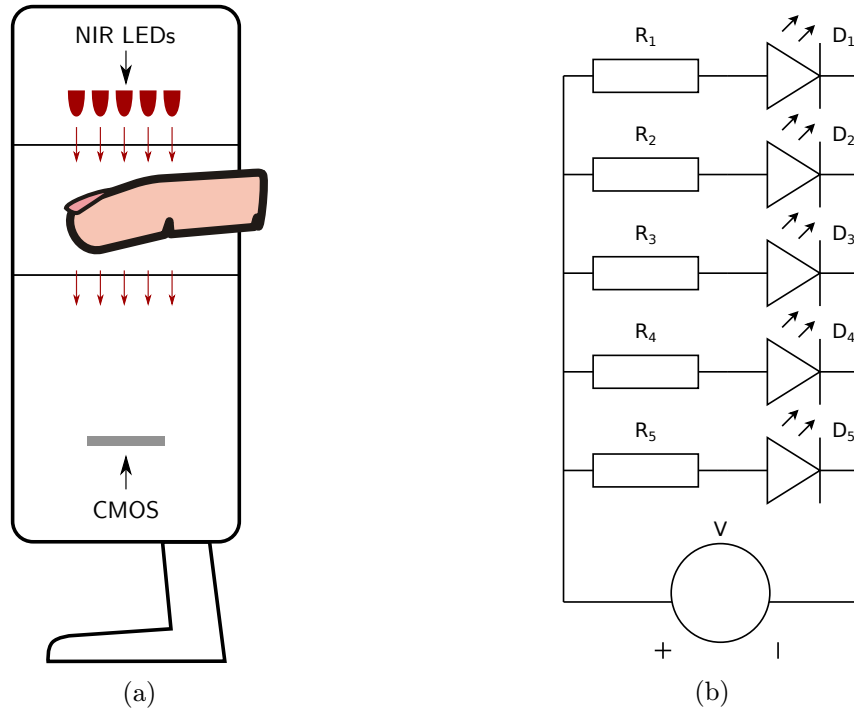


Figure 6.3: Proposed solution of finger vein sensing: (a) overall view; (b) wiring diagram of the extension circuit.

Together 26 different LEDs ranging from 405 nm to 955 nm were examined and some acquired images can be seen in [Figure 6.4](#). After that, a few LEDs settings were chosen to

be examined on several volunteers, and IR-870<sup>2</sup> was chosen for averagely giving the best results for different thicknesses of fingers. For full list of examined LEDs see [Table A.1](#).

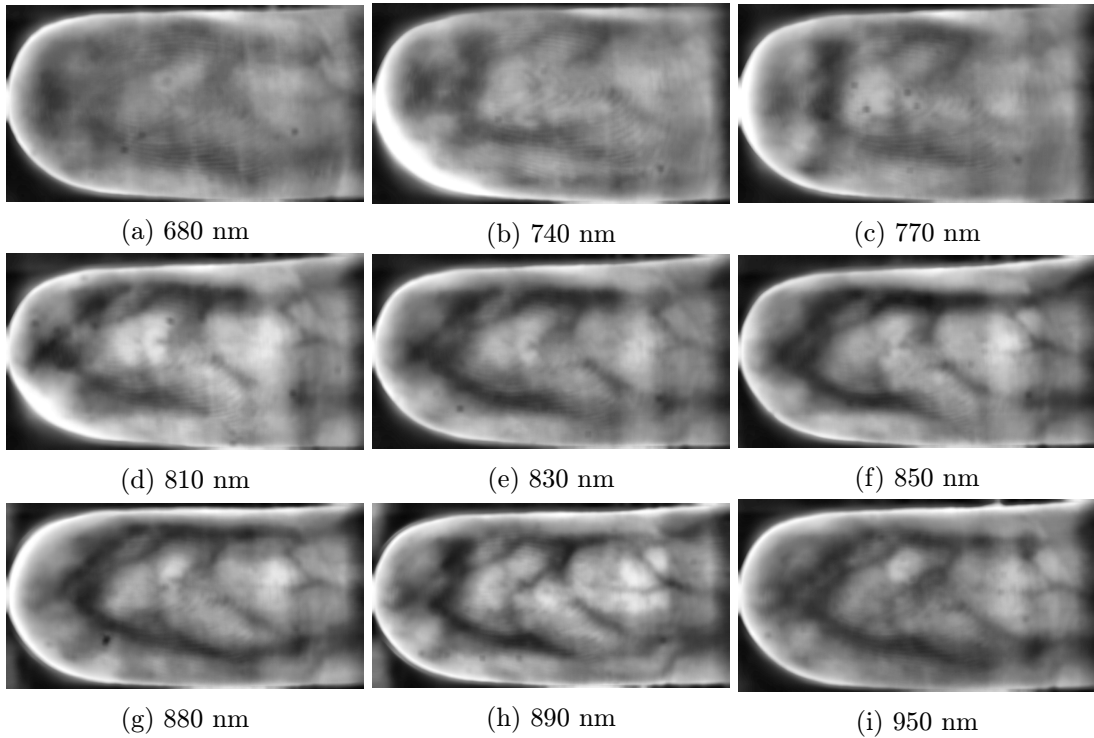


Figure 6.4: Examples of captured images of the same finger in different wavelengths. All images were enhanced using CLAHE to emphasize veins.

As mentioned, the various thickness of a finger makes difficulties with choosing a general camera settings. As can be seen in [Figure 6.5](#), when a thin (top row) finger is captured a shorter exposure time is needed in comparison to thicker ones (bottom row). A possible software solution combines images of the finger with different exposure times using High Dynamic Range Imaging (HDR) technique, which produces a single HDR image with greater dynamic range of luminosity. Different solution is to capture several images with various exposure times and then use quality evaluation algorithms to choose the best from image series. Since the camera had to be re-programmed each time the exposure time is changed, to capture a sequence of images takes several seconds, and therefore HDR approach could not be utilized due to possible finger posture changes. The second mentioned approach will be discussed in [Section 6.3](#).

## 6.2 Pre-processing

In this section, the pre-processing of the originally captured images will be presented. First, the image is segmented to obtain the finger mask, and after that the elimination of finger posture changes will be described.

<sup>2</sup><http://www.led-eshop.de/PDF/special/IR-870-T0-10NN.pdf>

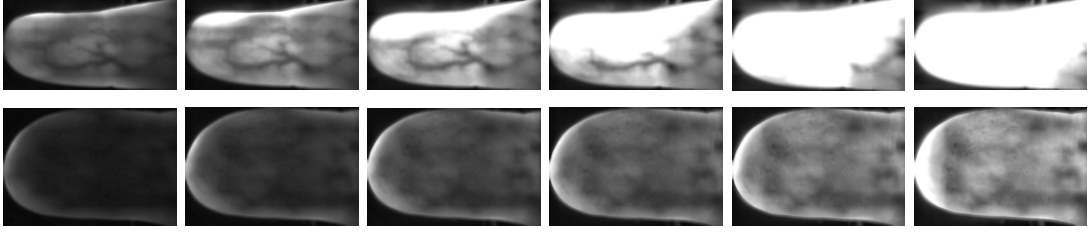


Figure 6.5: Finger vein images captured with different exposure times. In each row, there are images of the same finger and appropriate columns belong to the same exposure time. The exposure time grows in the right. All images were enhanced using CLAHE.

### 6.2.1 Region of Interest Localization

Conventional algorithms for finger vein ROI localization assume touch based sensor, and therefore the ROI of the finger is obtained by applying a fixed window mask. This straightforward approach cannot be used in most touchless systems, and therefore a method using Watershed for ROI localization will be introduced.

In [Figure 6.6a](#), example of an acquired upcropped image can be seen. The goal of the ROI localization is to distinguish between the finger and the background.

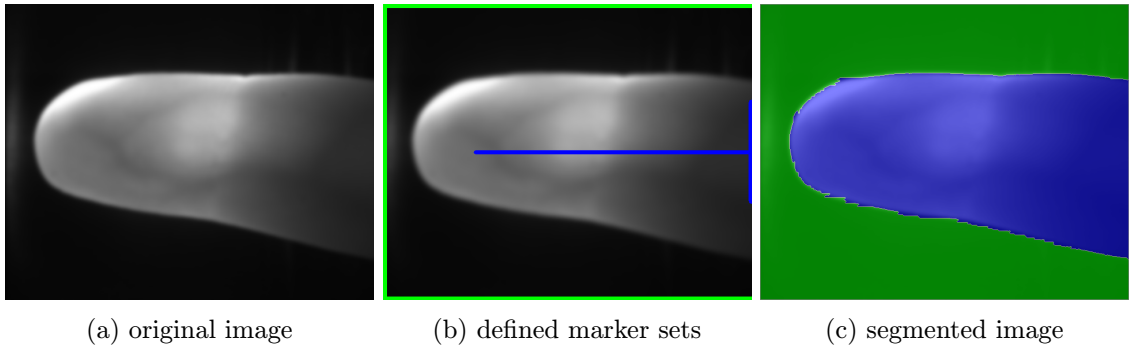


Figure 6.6: Example of Watershed procedure. ■  $W_f$ , ■  $W_b$ .

The Watershed algorithm was utilized to distinguish between the finger and the background. In order to use the Watershed algorithm, for all classes there must be preset a set of pixels, which belong to the appropriate class. Let us denote the image size as a tuple  $(x_m, y_m)$ . The background marker set  $W_b$  is defined using [Equation \(6.1\)](#) and the finger marker set  $W_f$  using [Equation \(6.2\)](#). Examples of predefined sets can be seen in [Figure 6.6b](#) and the result of the Watershed algorithm is displayed in [Figure 6.6c](#).

$$W_b = \{(1, y) \mid y \in \{1, \dots, y_m\}\} \cup \{(x, y) \mid x \in \{1, \dots, x_m\} \wedge y \in \{1, y_m\}\} \quad (6.1)$$

$$W_f = \{(x, y) \mid x \in \{\frac{1}{4}x_m, \dots, x_m\}, y = \frac{1}{2}y_m\} \cup \{(x_m, y) \mid y \in \{\frac{1}{3}y_m, \frac{2}{3}y_m\}\} \quad (6.2)$$

According to the segmented image, mask  $M(x, y)$  is defined, it returns 1 if  $(x, y)$  belongs to the finger segment, 0 otherwise. To reduce possible inaccuracies in segmentation, the morphological opening is applied on finger mask  $M$ , followed by morphological closing.

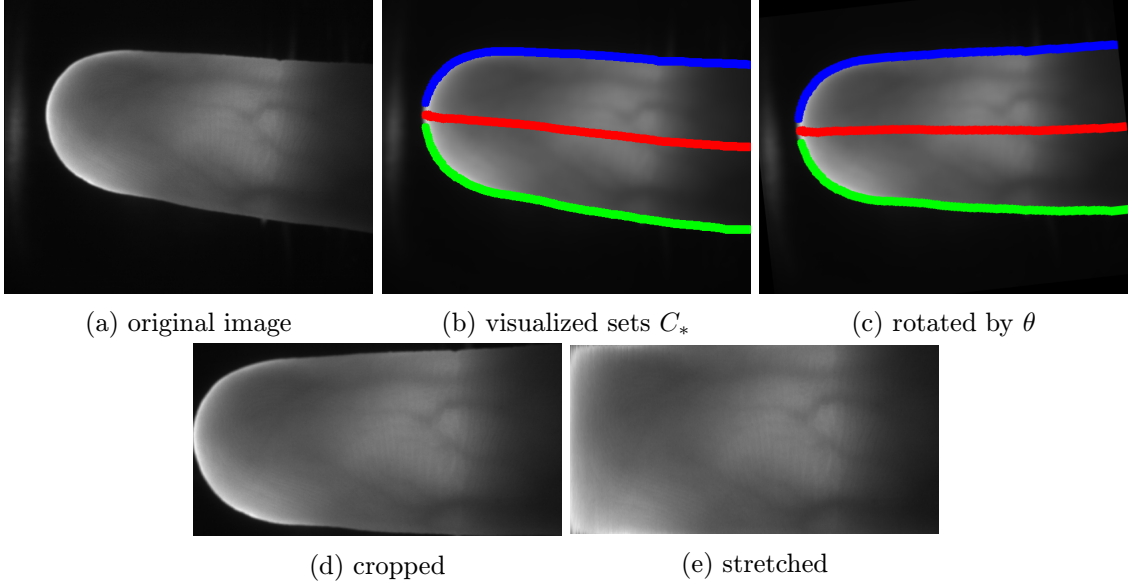


Figure 6.7: Procedure of elimination of finger posture changes. ■  $C_{top}$ , ■  $C_{bottom}$ , ■  $C_{middline}$  sets.

### 6.2.2 Correction of Finger Posture Changes

There are six basic finger posture changes described in [Section 5.3.2](#). In this section, the corrections and image normalization will be presented.

**Type 6 Correction** Type 6 finger posture change can be eliminated by rotation around the z-axis using rotation matrix  $R(\theta)$ . In order to obtain the unknown rotation  $\theta$ , sets  $C_{top}$  in [Equation \(6.3\)](#),  $C_{bottom}$  in [Equation \(6.4\)](#) and  $C_{middline}$  in [Equation \(6.5\)](#) are defined.

$$C_{top} = \{(x, y) \mid M(x, y) = 1 \wedge M(x, y - 1) = 0\} \quad (6.3)$$

$$C_{bottom} = \{(x, y) \mid M(x, y) = 1 \wedge M(x, y + 1) = 0\} \quad (6.4)$$

$$C_{middline} = \{(x, y) \mid \exists(x, y_T) \in C_{top} \wedge \exists(x, y_B) \in C_{bottom} \wedge y_B + y_T = 2y\}, \quad (6.5)$$

where  $M(x, y)$  is an image segmentation mask. Examples of these sets are visualized in [Figure 6.7b](#).

The  $C_{middline}$  set is then approximated by a line using least-square error method. The angle  $\theta$ , between the approximated line and the negative part of x-axis, is used to eliminate the Type 6 posture change. The result can be seen in [Figure 6.7c](#).

**Type 3 Correction** When the Type 6 posture change is eliminated, it is possible to crop the finger image according to the finger mask to minimize the image size while preserving the ROI. As a consequence, the Type 3 change is eliminated as well. This step is visualized in [Figure 6.7d](#).

**Type 1 Correction** The Type 1 posture change is trivially solved, since the position of the fingertip is known, and therefore alignment according to left border solves the Type 1 posture change.



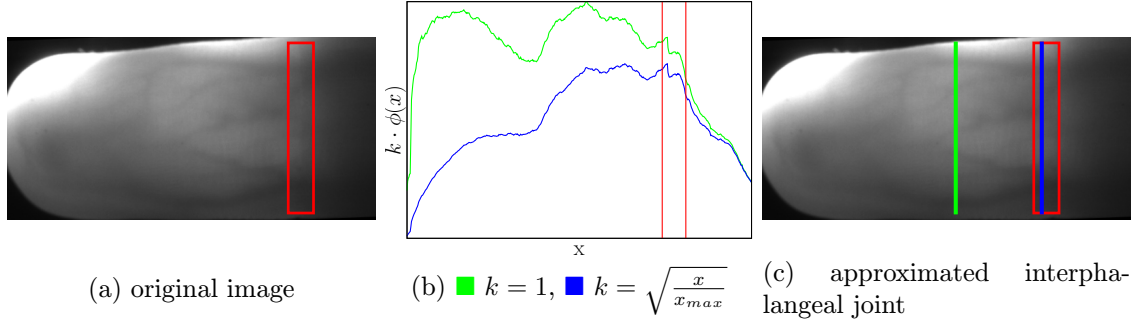


Figure 6.8: Interphalangeal joint localization. ■ Expected area of interphalangeal joint, ■ method for detection used in [25], ■ proposed method.

**Type 5 Correction** To eliminate Type 5 posture change, the finger vein image is normalized to a rectangle using a finger image mask. The image with size  $(x_{max}, y_{max})$  is separated by columns and each column segment, where  $M(x, y) = 1$  is linearly stretched to the size  $(1, y_{max})$ . The result of this operation is displayed in Figure 6.7e.

**Type 2 & 4** Both Type 2 and 4 posture changes are ignored in this work.

### 6.2.3 Interphalangeal Joint Localization

After Type 2 correction, it is possible to detect the interphalangeal joint. Experimentation with method described in Section 5.3.3 brought a promising result, but wrongly detected joints were also found as shown in Figure 6.8c. Better results were obtained using weighted  $\phi$  in Equation (6.6), where smaller weight is given with the length of the finger. This weighting is necessary, due to frequent wrong positioning of the users finger. The fingertip is then over-illuminated, and might cause wrongly localized interphalangeal joint. The comparison of the proposed method and method used in [25] is displayed in Figure 6.8.

$$r_k = \operatorname{argmax}_{x \in \{1, \dots, x_{max}\}} \left( \sqrt{\frac{x}{x_{max}}} \cdot \phi(x) \right) \quad (6.6)$$

The knowledge of approximation position of interphalangeal joint will be used in following size normalization.

### 6.2.4 Size Normalization

It is desired to have a feature vector of a constant size and this can be achieved by cropping the stretched image followed by scaling. For cropping, the  $r_k$  (interphalangeal joint approximation) is used as right border and  $\frac{r_k}{8}$  is used as a left border. The height of the image is preserved. After that the cropped image is scaled to size  $300 \times 200$  pixels.

## 6.3 Quality Assessment

Due to various thickness of fingers of different persons, it is necessary to acquire several images of the same finger with different exposure time as can be seen in Figure 6.5. Each finger vein record is contained of a totally ordered set  $V$  with *six* pictures. Further in the

text, this set will be denoted as a *sequence*. There exists a function  $e : V \rightarrow \mathbb{N}$ , which assigns each image an exposure time expressed as a natural number and  $e$  is totally ordered on  $V$ .

The quality estimation function  $q : V \rightarrow \mathbb{R}$  assigns a score to each image. After that, the image with best score  $I_{best}$  is chosen:  $I_{best} = \underset{v \in V}{\operatorname{argmax}} q(v)$  from the sequence. Several concrete quality estimation approaches can be utilized to choose the best quality image and its score from  $V$  and will be presented below.

**No Heuristic** Let us define a quality estimation  $NoHeuristic_i$ , which statically assigns 1 to the image with the  $i^{\text{th}}$  highest exposure time and 0 to others.

**Haralick** As described in [Section 5.3.5](#), Haralick features are also suited and successfully used, to estimate the image quality.  $Haralick_F^{(d,\theta)}$  is a quality estimation function, which assigns score to image according to selected Haralick feature  $F$ , where  $F \in \{Energy, Contrast, Homogeneity, Entropy\}$  and displacement vector  $(d, \theta)$ .

**Histogram Comparison** New approach using histogram comparison was also incorporated. An expert can choose a reference image, which histogram will be computed and other image's quality will be estimated by histogram comparison, for example using chi-square method.

Let us denote  $HComparison_k^p$  as quality estimation function, where  $k$  is a number of bins used in histogram computation and  $p$  is a constraint of the last bin (white color bin). Let us denote the height of the last bin as  $h_k$ . If  $h_k > p \cdot x_{max} \cdot y_{max}$ , then the image is penalized assigning its score according to [Equation \(6.7\)](#).

$$q = Q_{min} - \frac{h_k}{x_{max} \cdot y_{max}}, \quad (6.7)$$

where  $Q_{min}$  is the lowest possible score. This solution is aiming to detect over-illuminated images and give them penalty score according to the size of the over-illuminated.

## 6.4 Feature Extraction

The Haralick and LBPH features described in [Section 5.4](#) were utilized as a texture describing features, which will be mainly used as a discriminative features for liveness detection. In case of Haralick features, all four mentioned (contrast, energy, homogeneity, entropy) are concatenated to a single feature vector.

On the other hand, Maximum Curvature and Repeated Line Tracking are suited for detailed vein evaluation and therefore finger vein recognition. The outcome of both Maximum Curvature and Repeated Line Tracking is a locus space with probability of being a vein. This locus space is thresholded using threshold  $t$ , computed as  $t$ -percentil of non-zero locus space values. In case of Repeated Line Tracking, the parameters  $p_{lr}$  and  $p_{ud}$  were preset to  $p_{lr} = 0.5$  and  $p_{ud} = 0.25$ , because the veins are generally directing horizontally.

Examples of live fingers, finger falsifications and intermediate results of feature extraction step can be seen in [Figure 6.9](#). Note, that in both Repeated Line Tracking and Maximum Curvature method were veins found even in falsification samples.

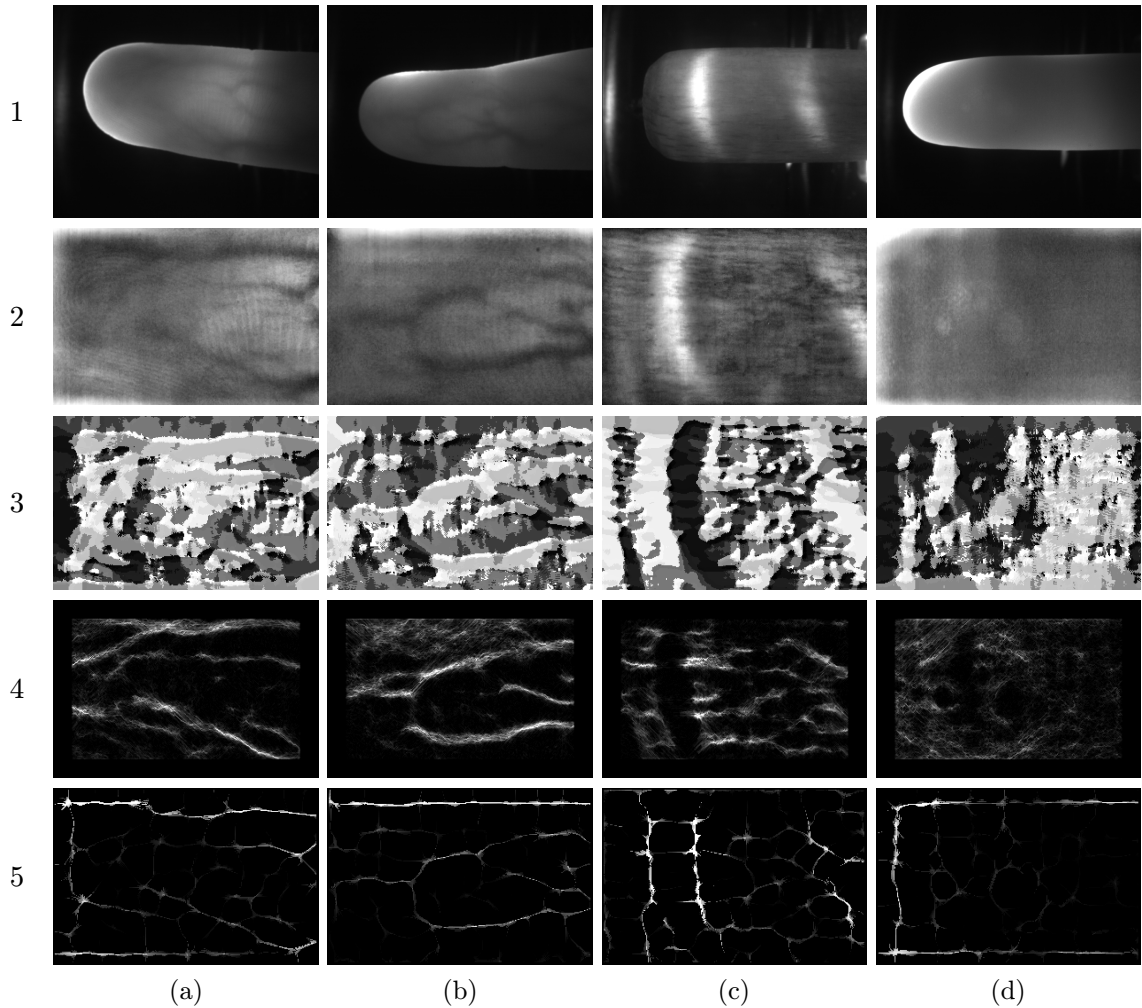


Figure 6.9: Examples of real fingers and finger falsifications and their intermediate results of feature extraction phase. Images in a column corresponds to the same sample: (a), (b) real fingers, (c) wooden falsification, (d) rubber falsification. In 1<sup>th</sup> row, there are originally acquired images. In 2<sup>nd</sup> row, there are normalized ROIs, after that in a 3<sup>rd</sup> row a  $LBP_{8,5}$ , next Repeated Line Tracking with configuration  $W = 31$ ,  $r = 5$  and 9,000 iterations in 4<sup>th</sup> row. In the 5<sup>th</sup> row there are outcomes of Maximum Curvature method.

## 6.5 Classification and Matching

The last step in processing pipeline is dependent on the chosen mode: liveness detection or vein recognition. In the classification mode, binary (with classes live and non-live) non-linear probabilistic SVM with RBF as a kernel is used for final decision.

The recognition mode details are dependent on used feature extraction method. To determine score of two LBPH vectors a chi-square metric is used. In case of Repeated Line Tracking and Maximum Curvature, the veins are aligned using ICP algorithm, after that the detected veins are emphasized with morphological operations and the final comparison score is based on Hamming Distance of intersectioning regions.

# Chapter 7

## Implementation

In this chapter, implementation details of the proposed finger liveness detection system are presented. The system can be divided into two subsystems: sensing and evaluation.

### 7.1 Sensing Subsystem

For actual work with the sensor (camera programming, build-in LEDs control, acquired image saving, etc.) a program *ProfileDeveloper* was used, which is an internal application of the TBS developer team. The application was adjusted for needs of experimentation and dataset collection. The acquired finger vein images are stored on a hard drive of a computer and then processed further by a evaluation subsystem.

It should be mentioned, that the sensing is not fully automated. After a finger is presented to the sensor a button in graphical user interface has to be pressed which starts the acquisition.

### 7.2 Evaluation Subsystem

For the sake of processing speed, the evaluation subsystem is implemented as a command line application in C++ language. It uses Bio FrameWork C++<sup>1</sup>, which was used to simplify feature extraction and performance evaluation. OpenCV<sup>2</sup> library was utilized for image processing. LibSVM<sup>3</sup> was used to train SVM, since it supports, in comparison to OpenCV version of SVM implementation, a probabilistic version. For ICP algorithm, a library libpointmatcher<sup>4</sup> was used.

The Repeated Line Tracking and Maximum Curvature sample Matlab codes<sup>5</sup> were re-implemented<sup>6</sup> to C++ using OpenCV as stand-alone libraries, so other researchers could use them and contribute.

The evaluation system loads and evaluates the whole dataset at once, so it is not possible to process single image. Using command line arguments, it is possible to choose the mode of the application, the quality assessment algorithm and the extracted feature vectors. The

---

<sup>1</sup><https://github.com/hadzim/BioFW>

<sup>2</sup><http://opencv.org/>

<sup>3</sup><http://www.csie.ntu.edu.tw/~cjlin/libsvm/>

<sup>4</sup><https://github.com/ethz-asl/libpointmatcher>

<sup>5</sup><http://mathworks.com/matlabcentral/fileexchange/35716-miura-et-al-vein-extraction-methods>

<sup>6</sup><https://github.com/dohnto/>

system automatically divides the dataset into several non-overlapping parts to perform cross-validation and finally display the results in both visual and textual form.

### 7.3 Quality Annotator

An application for manual quality annotation of finger vein was implemented for objective evaluation of quality assessment algorithms. It scans for all sets of six images from the same session and then it displays them on screen using QT framework<sup>7</sup>. An expert can then assign the images a label (good or bad) as can be seen in Figure 7.1. The output of quality annotator can be used in evaluation subsystem to evaluate different approaches of quality assessment.

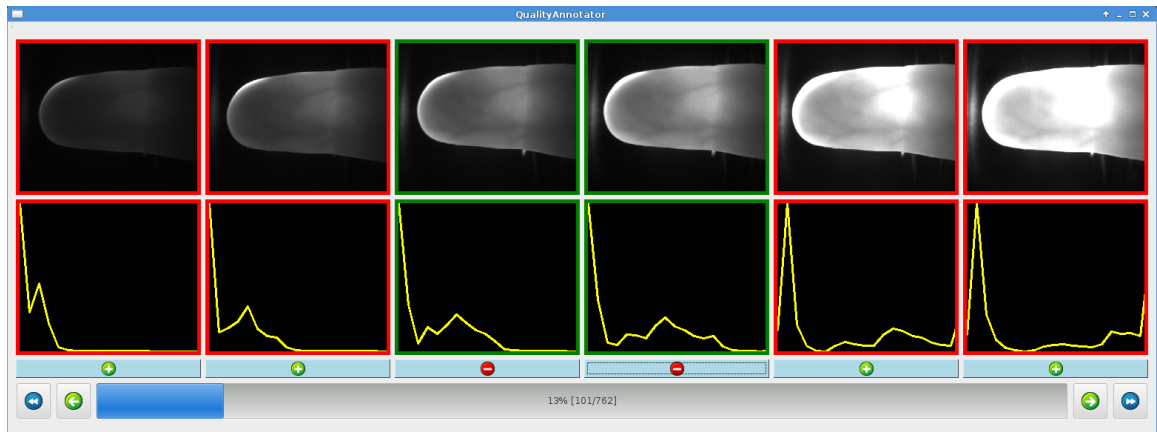


Figure 7.1: Screenshot of quality annotator application. The images highlighted with green color were marked as good, on the other hand images highlighted with red are marked as poor quality images.

---

<sup>7</sup><http://www.qt.io/>

# Chapter 8

## Evaluation

In this chapter, an evaluation of the proposed system is discussed. First, a gathered dataset is described. After that, quality assessment approaches are compared using manually annotated dataset. Next, both liveness detection and finger vein recognition modes of the proposed system are evaluated. Last but not least, a future work leading to possible performance improvement is outlined.

### 8.1 Dataset Description

To evaluate the proposed system, a dataset containing both live fingers and fingers falsifications was gathered. 23 volunteers were willing to provide their fingers for this purpose. Six fingers (both index, middle and ring fingers) of each volunteer were captured and each finger can be perceived as a biometric sample of a unique individual. Each finger was captured six times in two different days to take into account possible changes of vein visibility. Together 763 finger vein sequences were acquired (not all volunteers were able to provide all their fingers for sensing from various reasons). The volunteers were instructed to always put their finger to approximately the same position, but often variations in finger posture happened.

The non-live dataset consists of 370 sequences of 59 different materials or material combinations. Examples of items in non-live dataset fingers can be seen in [Figure 8.1](#).

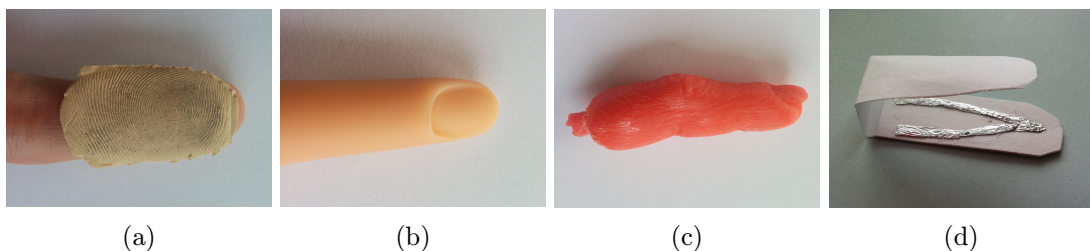


Figure 8.1: Example items of non-live dataset: (a) real finger with a thin layer of a milk latex as a fake fingerprint; (b) finger from rubber; (c) finger printed using 3D-printer; (d) paper finger with aluminum foil as veins and a dispersion layer.

## 8.2 Quality Assessment

First, the quality assessment approaches will be compared. Using quality annotator application, 200 image sequences (1,200 images in total) were manually annotated into two classes: good quality and poor quality. The poor quality set is usually consisted of images where no veins are visible and images with large over-illuminated areas. The goal of the quality assessment is to choose the most high-contrasted, best quality, not over-illuminated image from the six images from the sequence.

The results of all approaches with selected configurations can be seen in table [Table 8.1](#). Using *NoHeuristic* with static choice 2 can give promising results. On the other hand, Haralick features do not seem to be a good criteria in this case. The best results were obtained using energy feature, but the results are inferior in comparison to using static *NoHeuristic*<sub>2</sub>. Both contrast and homogeneity failed to distinguish between two annotated classes probably due to over-illuminated segments, which were labeled as a poor quality by the expert. Possible explanation is, that in other research papers Haralick features were used to distinguish between images with visible and barely visible veins, however we utilize it also to discriminate between over-illuminated images.

Table 8.1: Quality assessment methods comparison.

Method	Success Rate [%]	Method	Success Rate [%]
<i>NoHeuristic</i> <sub>1</sub>	39.5	<i>Haralick</i> <sup>(5,0)</sup> <sub>Contrast</sub>	34.0
<i>NoHeuristic</i> <sub>2</sub>	<b>72.5</b>	<i>Haralick</i> <sup>(10,90°)</sup> <sub>Energy</sub>	59.5
<i>NoHeuristic</i> <sub>3</sub>	49.0	<i>Haralick</i> <sup>(1,0)</sup> <sub>Homogeneity</sub>	25.5
<i>NoHeuristic</i> <sub>4</sub>	27.0	<i>HComparison</i> <sub>5</sub> <sup>0.05</sup>	<b>94.5</b>
<i>NoHeuristic</i> <sub>5</sub>	11.0	<i>HComparison</i> <sub>5</sub> <sup>0.1</sup>	90.5
<i>NoHeuristic</i> <sub>6</sub>	7.5	<i>HComparison</i> <sub>10</sub> <sup>0.05</sup>	88.0

The best result 94.5% was provided using histogram comparison method, which was mainly achieved due to incorporating the white bin threshold, which filters possible over-illuminated images. Similar extension to standard Haralick features could cause performance improvement as well.

Further in the evaluation, the *HComparison*<sub>5</sub><sup>0.05</sup> method will be used implicitly.

## 8.3 Liveness Detection

In this section, performance evaluation of liveness detection mode will be presented. Both (live and non-live datasets) are divided into five non-overlapping parts and then merged pairwise resulting into five sub-datasets with equally distributed live and non-live samples. After that, one sub-dataset is selected for evaluating the results and the remaining four are merged to train a non-linear probabilistic SVM with RBF kernel. The SVM is trained using cross-validation, where the training sub-dataset is again divided into five parts in order to find the best configuration. The performance is evaluated using the evaluation sub-dataset, which is submitted to SVM, which returns probability (since probabilistic version of SVM was incorporated) of being a live sample. This procedure is repeated five times, where evaluation sub-dataset is rotated and the results are merged together and presented below.

In case of Haralick features, three different angles  $\theta$  of displacement vector were examined:  $0^\circ$ ,  $45^\circ$  and  $90^\circ$ . The best results were obtained using  $90^\circ$ , probably due to finger orientation – most veins are directing to the length of the finger, and therefore using angle perpendicular to the vein can give more information about the gray level intensity transitions. On the other hand,  $0^\circ$  leads to the worst results. Lowest value of EER (13.0%) was obtained using displacement vector  $(3, 90^\circ)$ . Detailed results using Haralick features can be seen in [Figure 8.2a](#).

Extended LBP with various configurations were utilized in LBPH features. LBPH was examined with different number of regions. Generally, the best results were obtained using division into  $8 \times 8$  regions. EER equal to 6.5% was achieved using  $LBP_{8,1}$  with mentioned number of regions. Selected results using LBPH features can be seen in [Figure 8.2b](#).

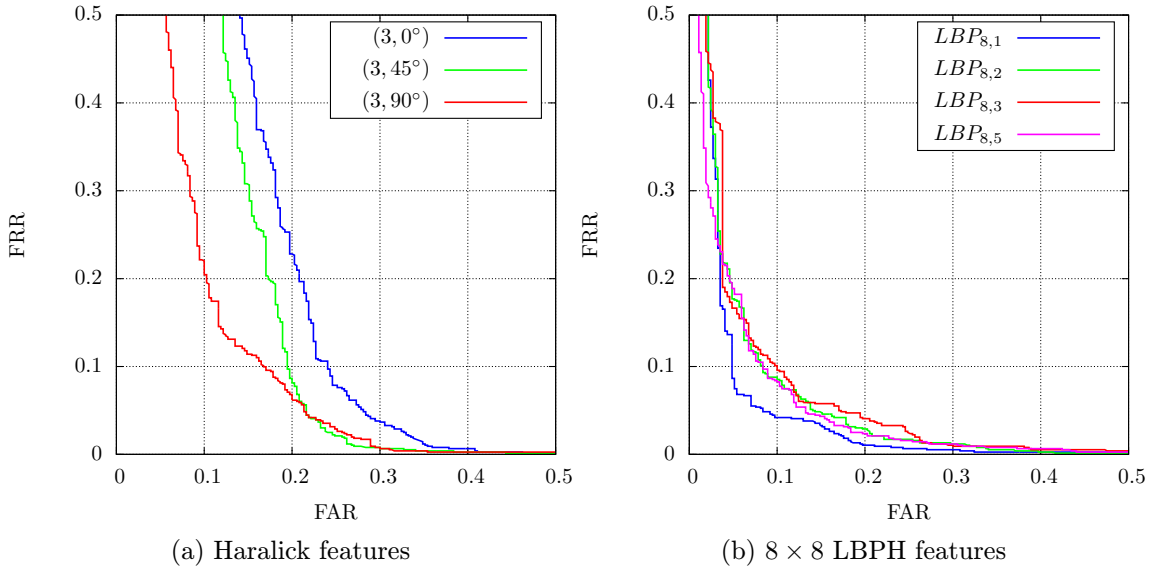


Figure 8.2: ROC curves for liveness detection mode with both (a) Haralick and (b) LBPH features with selected settings.

From the visualized ROC curves we can see, there are items in the non-live dataset, which have similar texture as a real finger and are classified into live class. These spoofing materials might be good candidates for producing a fake fingerprint, which could not be detected by the proposed liveness detection system. To items, repeatedly recognized as live, belong:

- real finger wearing a latex glove,
- real finger with thin layer of havel composite,
- real finger with thin layer of siloflex.

In case of the first two mentioned materials, infrared light penetrates through the material heavily, and therefore veins of the real finger are still visible as displayed in [Figure 8.3](#). The siloflex in combination with real finger hides the veins, but creates an illusion of a thick finger with hardly visible veins. As we can see, the texture based approach can be defeated using appropriate materials for fingerprint falsifications.

The texture based approach could be extended to extract veins and compare them to appropriate user template. Results of such approach will be presented in next section.



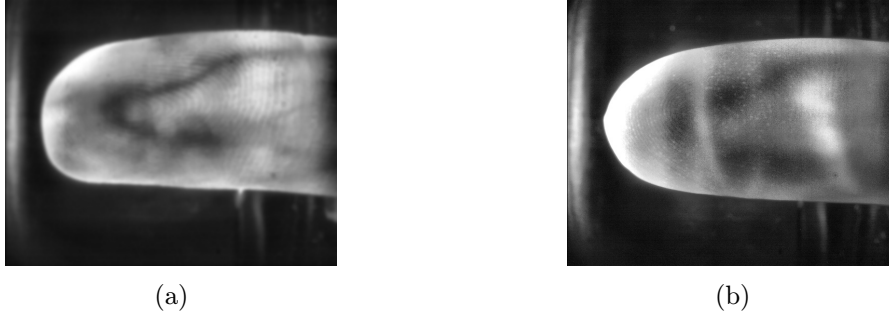


Figure 8.3: Example of using semi-transparent latex glove: (a) real finger; (b) same finger with latex glove. Both images were enhanced using CLAHE.

## 8.4 Finger Vein Recognition

In this section, the performance of finger vein recognition mode will be evaluated. The live dataset is divided into six non-overlapping parts. Single sub-dataset is used to create user templates and the rest (five sub-datasets of live dataset and whole non-live dataset) is used for matching against the templates. This procedure is repeated six times, rotating the template dataset and the results are merged together and presented below.

First, the LBPH were examined using several window divisions and LBP parameters. The best result, EER equal to 19.5%, was obtained using  $LBP_{8,2}$  with  $8 \times 8$  regions. Selected results are depicted in [Figure 8.4a](#). As we can see, the LBPH features are not suitable for detailed vein matching.

Repeated Line Tracking method seems to be superior to LBPH, because EER of 15.1% was achieved with 9,000 iterations,  $r = 1$ ,  $W = 31$  and  $t = 70$ . 9,000 iterations seem to be sufficient to distinguish between noise and veins. It should be noted, that this approach is highly time consuming in comparison to other methods and the results are still poor.

Best results were obtained using Maximum Curvature extraction method. Selected ROC curves can be seen in [Figure 8.4](#). The lowest EER of 10.8% was achieved using threshold  $t = 60$ . It should be mentioned, that presented results were obtained without contrast enhancement. On the contrary, if CLAHE was utilized, the EER value increases of 3%. The Maximum Curvature method is able to deal with vein localization even without contrast enhancement and mentioned enhancement negatively emphasize noise.

The results are far from perfect. The main reason for such outcome is unstable finger posture of users as depicted in [Figure 8.5](#). As a consequence, different veins become visible or on the other hand become hardly distinguishable. This problem could be solved using an automatic sensing unit, which would detect correct finger posture and acquire image. In this case, an automatic brightness control could be utilized as well. Remaining two cameras to reconstruct a 3D model of the blood vessels could be utilized to increase a performance of the proposed system. Unfortunately, all these extension are not trivial and hardware changes has to be made.

## 8.5 Concluding Remarks

The proposed system is a proof of concept prototype showing potential of finger vein recognition. The experimental results show, that more work has to be done before integrating

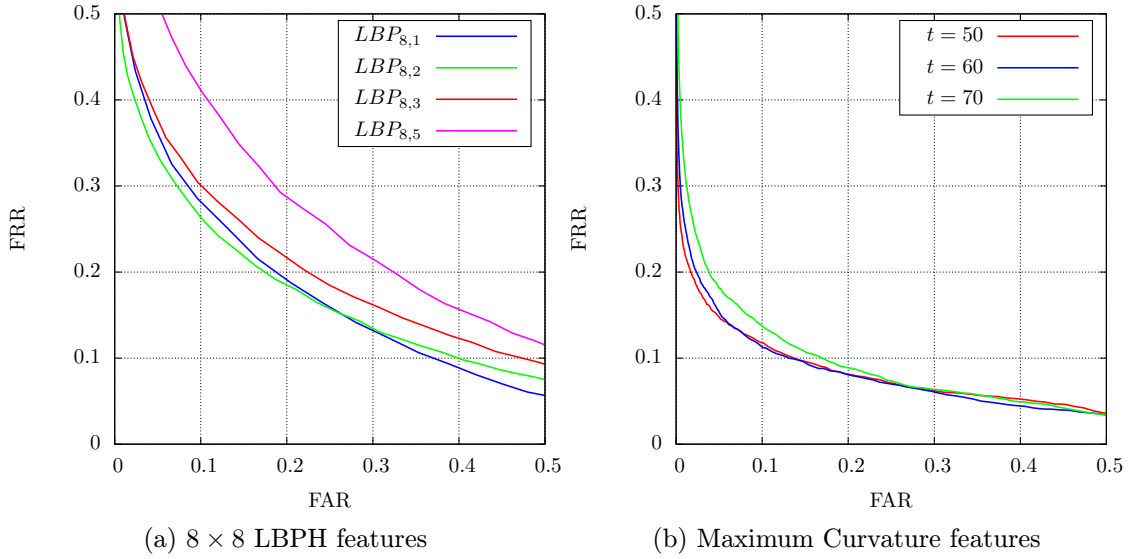


Figure 8.4: Resulting ROC curves for finger vein recognition mode with selected settings.

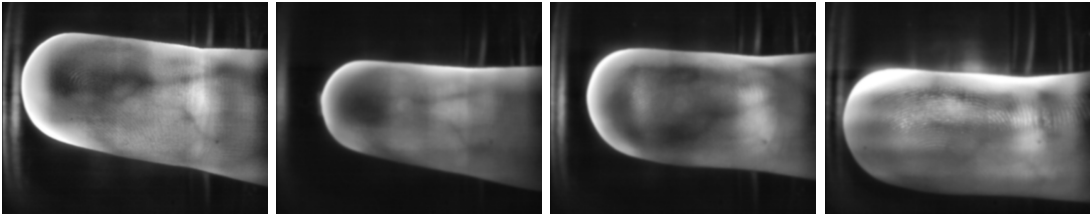


Figure 8.5: Examples of images of the same finger from different sessions of user with hardly visible vein and unstable finger posture. All images were enhanced using CLAHE.

into a TBS sensor for real usage is possible.

The future development of the system include following tasks. Two lines of LEDs instead of one could be used. These could be mounted to the top side corners or to the sides of the box, and this would allow to use additional two cameras. This step would allow to reconstruct a 3D blood vessel model of a user. Also, utilization of HDR method could be beneficial. However, it would require additional changes to sensing module. Last but not least, fully automatic sensing and brightness control could lead to more uniform illumination and stable finger postures.

## Chapter 9

# Conclusion

Fingerprint recognition is well known and established method suitable for biometric authentication. Lately, the spoofing attacks have shown that it is possible to fool most commercial fingerprint sensors with artificial fingerprints. On the contrary, finger vein recognition is a relatively new but promising method suitable for biometric authentication achieving high recognition performance. One advantage of vein recognition is that blood vessels are an internal biometric characteristic and it is harder for an attacker to obtain it from a user. Image of veins is usually acquired using infrared radiation for biometric purposes. When we create a biometric system, which examines both mentioned characteristics at once, it is more demanding to compromise it. An intruder has to obtain both fingerprint and image of finger veins of a legitimate user and merge those into a single falsification, which has desired optical characteristics.

The goal of this thesis was to design and implement a liveness detection system based on finger vein pattern and extend an existing fingerprint solution. First, I studied literature concerning fingerprint recognition, various liveness detection approaches on fingers and finger vein recognition related algorithms. I have chosen to extend commercial Touchless Biometric Systems 3D-Enroll fingerprint sensor. I proposed and realized a hardware solution using infrared radiation with transmission setup. Using constructed sensor I gathered a dataset containing more than 1,100 records including both real fingers and finger falsifications.

I proposed and successfully utilized a quality assessment algorithm, which deals with various thicknesses of fingers. Also, I designed and implemented software for fully automatic evaluation of liveness detection and finger vein verification.

All implemented methods were thoroughly evaluated and compared. In liveness detection mode, EER equal to 6.5% was achieved using LBPH features. In finger vein verification mode, the best result EER equal to 10.8% was obtained using Maximum Curvature features. A future development, which may improve the error rates, was outlined including reconstruction of 3D model of blood vessels.

As we can see, the error rates are quite high for unimodal system, but in fusion with high precision fingerprint recognition, it might be possible to preclude most of impostor attempts without rejecting any legitimate user.

# Bibliography

- [1] ISO/IEC. *ISO/IEC 2382-37. Information technology – Vocabulary – Biometrics*. ISO/IEC, 2012.
- [2] JAIN, A. K., FLYNN, P., AND ROSS, A. A. *Handbook of Biometrics*. Springer-Verlag New York, Inc., Secaucus, NJ, USA, 2007. ISBN: 978-0387710402.
- [3] HARTUNG, D. *Vascular Pattern Recognition and its Application in Privacy-Preserving Biometric Online-Banking Systems*. PhD thesis, Gjøvik University College, 2012. ISBN: 978-82-93269-01-4.
- [4] DRAHANSKÝ, M., ORSÁG, F., AND DOLEŽEL, M. *Biometrie*. Computer Press, 2011. ISBN: 978-80-254-8979-6.
- [5] ROSS, A., AND JAIN, A. Multimodal biometrics: An overview. In *Proc. of 12th European Signal Processing Conference (EUSIPCO)* (2004), pp. 1221–1224.
- [6] SANDSTRÖM, M. *Liveness Detection in Fingerprint Recognition Systems*. PhD thesis, Linköping University, 2004. Available at:  
<http://www.diva-portal.org/smash/get/diva2:19729/FULLTEXT01.pdf>.
- [7] GRAY, H., AND LEWIS, W. H. *Anatomy of the human body*. Philadelphia, Lea & Febiger, 1918. Available at:  
<http://www.biodiversitylibrary.org/bibliography/20311>.
- [8] KÜCKEN, M., AND NEWELL, A. C. Fingerprint formation. *Journal of theoretical biology* 235, 1 (2005), pp. 71–83. ISSN: 0022-5193.
- [9] FENG, J., JAIN, A. K., AND ROSS, A. Fingerprint alteration. Tech. Rep. MSU-CSE-09-30, Department of Computer Science, Michigan State University, East Lansing, Michigan, December 2009.
- [10] THALHEIM, L., AND KRISLER, J. Body check: Biometric access protection devices and their programs put to the test. *c't magazine* (November 2002). ISSN: 0724-8679.
- [11] PARZIALE, G. *Advances in biometrics: sensors, systems and algorithms*. Springer, 2007. ISBN: 978-1-84628-921-7.
- [12] SHAH, J., AND POSHIYA, U. Touchless fingerprint recognition. *Asian Journal of Computer Science & Information Technology* 3, 5 (2013). ISSN : 2249-5126.
- [13] MALTONI, D., MAIO, D., JAIN, A., AND PRABHAKAR, S. *Handbook of Fingerprint Recognition*. Springer Professional Computing. Springer London, 2009. ISBN: 978-1-84882-254-2.

- [14] BAZEN, A. M. *Fingerprint Identification - Feature Extraction, Matching and Database Search*. PhD thesis, University of Twente, Enschede, the Netherlands, September 2002. ISBN: 9036517818.
- [15] DRAHANSKY, M. Liveness detection in biometrics. In *Advanced Biometric Technologies*. InTech, 2011, pp. 179–198. ISBN: 978-953-307-487-0. Available at: <http://www.intechopen.com/books/advanced-biometric-technologies/liveness-detection-in-biometrics>.
- [16] DERAKHSHANI, R., SCHUCKERS, S. A., HORNAK, L. A., AND O’GORMAN, L. Determination of vitality from a non-invasive biomedical measurement for use in fingerprint scanners. *Pattern Recognition* 36, 2 (2003), pp. 383 – 396. ISSN: 0031-3203.
- [17] PRAHL, S. Optical Absorption of Hemoglobin, Dec. 1999 [Accessed: 2015-05-13]. Available at: <http://omlc.ogi.edu/spectra/hemoglobin/>.
- [18] DRAHANSKÝ, M., DOLEŽEL, M., VÁŇA, J., BŘEZINOVÁ, E., YIM, J., AND SHIM, K. New optical methods for liveness detection on fingers. *BioMed Research International* 2013, 9 (2013), pp. 1–11. ISSN: 2314-6133. Available at: <http://www.hindawi.com/journals/bmri/2013/197925/>.
- [19] BIN, Q., JIAN-FEI, P., GUANG-ZHONG, C., AND GE-GUO, D. The anti-spoofing study of vein identification system. In *Computational Intelligence and Security, 2009. CIS '09. International Conference on* (Dec 2009), vol. 2, pp. 357–360. ISBN: 978-1-4244-5411-2.
- [20] FUKSIS, R., GREITANS, M., NIKISINS, O., AND PUDZS, M. Infrared imaging system for analysis of blood vessel structure. *Elektronika ir Elektrotechnika* 97, 1 (2010), pp. 45–48. ISSN: 2029-5731.
- [21] ANDERSON, R. R., AND PARRISH, J. A. The optics of human skin. *Journal of Investigative Dermatology* 77, 1 (1981), pp. 13–19. ISSN: 0022-202X.
- [22] ZHANG, C., LI, X., LIU, Z., ZHAO, Q., XU, H., AND SU, F. The cfvd reflection-type finger-vein image database with evaluation baseline. In *Biometric Recognition*, Z. Sun, S. Shan, G. Yang, J. Zhou, Y. Wang, and Y. Yin, Eds., vol. 8232 of *Lecture Notes in Computer Science*. Springer International Publishing, 2013, pp. 282–287. ISBN: 978-3-319-02960-3.
- [23] HASHIMOTO, J. Finger vein authentication technology and its future. In *VLSI Circuits, 2006. Digest of Technical Papers. 2006 Symposium on* (2006), pp. 5–8. ISBN: 1-4244-0006-6.
- [24] YANG, J., AND SHI, Y. Towards finger-vein image restoration and enhancement for finger-vein recognition. *Information Sciences* 268 (2014), pp. 33–52. ISSN: 0020-0255.
- [25] YANG, J., AND SHI, Y. Finger-vein roi localization and vein ridge enhancement. *Pattern Recognition Letters* 33, 12 (2012), pp. 1569–1579. ISSN: 0167-8655.

- [26] XI, X., YANG, G., YIN, Y., AND MENG, X. Finger vein recognition with personalized feature selection. *Sensors* 13, 9 (2013), pp. 11243–11259. ISSN: 2333-9721.
- [27] LIU, Z., YIN, Y., WANG, H., SONG, S., AND LI, Q. Finger vein recognition with manifold learning. *Journal of Network and Computer Applications* 33, 3 (2010), pp. 275–282. ISSN: 1084-8045.
- [28] LEE, E. C., AND PARK, K. R. Image restoration of skin scattering and optical blurring for finger vein recognition. *Optics and Lasers in Engineering* 49, 7 (2011), pp. 816–828. ISSN: 0143-8166.
- [29] WU, J.-D., AND YE, S.-H. Driver identification using finger-vein patterns with radon transform and neural network. *Expert Systems with Applications* 36, 3 (2009), pp. 5793–5799. ISSN: 0957-4174.
- [30] NGUYEN, D. T., PARK, Y. H., SHIN, K. Y., KWON, S. Y., LEE, H. C., AND PARK, K. R. Fake finger-vein image detection based on fourier and wavelet transforms. *Digital Signal Processing* 23, 5 (2013), pp. 1401–1413. ISSN: 1051-2004.
- [31] CHUNYI, L., MINGZHONG, L., AND XIAO, S. A finger vein recognition algorithm based on gradient correlation. *AASRI Procedia* 1 (2012), pp. 40–45. ISSN: 2212-6716.
- [32] TON, B. T., AND VELDHUIS, R. N. A high quality finger vascular pattern dataset collected using a custom designed capturing device. In *Biometrics (ICB), 2013 International Conference on* (2013), IEEE, pp. 1–5. ISBN: 978-1-4799-0310-8.
- [33] LU, Y., XIE, S. J., YOON, S., WANG, Z., AND PARK, D. S. An available database for the research of finger vein recognition. In *Image and Signal Processing (CISP), 2013 6th International Congress on* (Dec 2013), vol. 01, pp. 410–415. ISBN: 978-1-4799-2763-0.
- [34] RAGHAVENDRA, R., RAJA, K., SURBIRYALA, J., AND BUSCH, C. A low-cost multimodal biometric sensor to capture finger vein and fingerprint. In *Biometrics (IJCB), 2014 IEEE International Joint Conference on* (Sept 2014), pp. 1–7. ISBN: 978-1-4799-3585-7.
- [35] YANG, W., HUANG, X., ZHOU, F., AND LIAO, Q. Comparative competitive coding for personal identification by using finger vein and finger dorsal texture fusion. *Information Sciences* 268 (2014), pp. 20–32. ISSN: 0020-0255.
- [36] MEYER, F. Color image segmentation. In *International Conference on Image Processing and its Applications* (1992), pp. 303–306. ISBN: 0-85296-543-5.
- [37] HUANG, B., LIU, S., AND LI, W. A finger posture change correction method for finger-vein recognition. In *Computational Intelligence for Security and Defence Applications (CISDA), 2012 IEEE Symposium on* (July 2012), pp. 1–7. ISBN: 978-1-4673-1416-9.
- [38] HUANG, B., DAI, Y., LI, R., TANG, D., AND LI, W. Finger-vein authentication based on wide line detector and pattern normalization. In *Pattern Recognition (ICPR), 2010 20th International Conference on* (2010), IEEE, pp. 1269–1272. ISBN: 978-1-4244-7542-1.

- [39] ZUIDERVELD, K. Contrast limited adaptive histogram equalization. In *Graphics Gems IV*, P. S. Heckbert, Ed. Academic Press Professional, Inc., San Diego, CA, USA, 1994, pp. 474–485. ISBN: 0-12-336155-9.
- [40] GOH KAH ONG MICHAEL, TEE CONNIE, A. B. J. T. In *Advanced Biometric Technologies*. 2011 [Accessed: 2015-05-13], ch. A Contactless Biometric System Using Palm Print and Palm Vein Features. Available at: <http://www.intechopen.com/books/advanced-biometric-technologies/a-contactless-biometric-system-using-palm-print-and-palm-vein-features>.
- [41] YANG, L., YANG, G., YIN, Y., AND XIAO, R. Finger vein image quality evaluation using support vector machines. *Optical Engineering* 52, 2 (2013). ISSN: 0091-3286.
- [42] IACOVIELLO, F., AND SUSMEL, L. *Frattura ed Integrità Strutturale: Annals 2011*. Annali della rivista IGF. IGF-Gruppo Italiano Frattura, 2011. ISBN: 978-8-895-94042-7.
- [43] PARK, K. R. Finger vein recognition by combining global and local features based on svm. *Computing and Informatics* 30, 2 (2011), pp. 295–309. ISSN: 1335-9150.
- [44] AHONEN, T., MATAS, J., HE, C., AND PIETIKÄINEN, M. Rotation invariant image description with local binary pattern histogram fourier features. In *Proceedings of the 16th Scandinavian Conference on Image Analysis* (Berlin, Heidelberg, 2009), SCIA '09, Springer-Verlag, pp. 61–70. ISBN: 978-3-642-02229-6.
- [45] AHONEN, T., HADID, A., AND PIETIKAINEN, M. Face description with local binary patterns: Application to face recognition. *Pattern Analysis and Machine Intelligence, IEEE Transactions on* 28, 12 (Dec 2006), pp. 2037–2041. ISSN: 0162-8828.
- [46] YANG, Z., AND AI, H. Demographic classification with local binary patterns. In *Advances in Biometrics*, S.-W. Lee and S. Li, Eds., vol. 4642 of *Lecture Notes in Computer Science*. Springer Berlin Heidelberg, 2007, pp. 464–473. ISBN: 978-3-540-74548-8.
- [47] ROSDI, B. A., SHING, C. W., AND SUANDI, S. A. Finger vein recognition using local line binary pattern. *Sensors* 11, 12 (2011), pp. 11357–11371. ISSN: 1424-8220.
- [48] PANG, S., YIN, Y., YANG, G., AND LI, Y. Rotation invariant finger vein recognition. In *Biometric Recognition*, W.-S. Zheng, Z. Sun, Y. Wang, X. Chen, P. Yuen, and J. Lai, Eds., vol. 7701 of *Lecture Notes in Computer Science*. Springer Berlin Heidelberg, 2012, pp. 151–156. ISBN: 978-3-642-35135-8.
- [49] MIURA, N., NAGASAKA, A., AND MIYATAKE, T. Feature extraction of finger-vein patterns based on repeated line tracking and its application to personal identification. *Mach. Vision Appl.* 15, 4 (Oct. 2004), pp. 194–203. ISSN: 0932-8092.
- [50] MIURA, N., NAGASAKA, A., AND MIYATAKE, T. Extraction of finger-vein patterns using maximum curvature points in image profiles. *IEICE - Trans. Inf. Syst. E90-D*, 8 (Aug. 2007), pp. 1185–1194. ISSN: 0916-8532.
- [51] ZHANG, H., LIU, Z., ZHAO, Q., ZHANG, C., AND FAN, D. Finger vein recognition based on gabor filter. In *Intelligence Science and Big Data Engineering*, C. Sun,

F. Fang, Z.-H. Zhou, W. Yang, and Z.-Y. Liu, Eds., vol. 8261 of *Lecture Notes in Computer Science*. Springer Berlin Heidelberg, 2013, pp. 827–834. ISBN: 978-3-642-42056-6.

- [52] HSU, C.-W., CHUNG CHANG, C., AND JEN LIN, C. A practical guide to support vector classification, 2010 [Accessed: 2015-05-13]. Available at: <http://www.csie.ntu.edu.tw/~cjlin/papers/guide/guide.pdf>.
- [53] BESL, P. J., AND MCKAY, N. D. A method for registration of 3-d shapes. *IEEE Trans. Pattern Anal. Mach. Intell.* 14, 2 (Feb. 1992), pp. 239–256. ISSN: 0162-8828.



# Acronyms

AHE . . . . .	Adaptive Histogram Equalization
ATM . . . . .	Automated Teller Machine
CCD . . . . .	Charge Coupled Device
CLAHE . . . . .	Contrast Limited Adaptive Histogram Equalization
CMOS . . . . .	Complementary Metal Oxide Semiconductor
DET . . . . .	Detection Error Tradeoff
DF . . . . .	Directional Field
EER . . . . .	Equal Error Rate
FA . . . . .	False Accept
FAR . . . . .	False Accept Rate
FMR . . . . .	False Match Rate
FNMR . . . . .	False Non-Match Rate
FR . . . . .	False Reject
FRR . . . . .	False Reject Rate
FTA . . . . .	Failure to Acquire
FTE . . . . .	Failure to Enroll
GLCM . . . . .	Gray Level Co-occurrence Matrix
HDR . . . . .	High Dynamic Range Imaging
ICP . . . . .	Iterative Closest Points
IR . . . . .	Infrared
LBP . . . . .	Local Binary Patterns

LBPH . . . . .	Local Binary Patterns Histogram
LED . . . . .	Light-Emitting Diode
NIR . . . . .	Near Infrared
PIFS . . . . .	Partitioned Iterated Function System
RBF . . . . .	Radial Basis Function
RDC . . . . .	Relative Dielectric Constant
ROC . . . . .	Receiver Operating Characteristic
ROI . . . . .	Region of Interest
SP . . . . .	Singularity Point
STRESS . . . . .	Spatio-Temporal Retinex-like Envelope with Stochastic Sampling
SVM . . . . .	Support Vector Machine
TBS . . . . .	Touchless Biometric Systems
UV . . . . .	Ultraviolet

# Appendix A

## Tables

Table A.1: List of examined LEDs for finger vein acquisition using transmission method.

Producer	Type	Color	Wavelength [nm]
OptoSupply	OSSV5131A	Ultraviolet (UV)	405
–	–	blue	–
OptoSupply	OSG58A5111A	green	525
OptoSupply	OSYL5111A-TU	yellow	590
OptoSupply	OSPW5111A-Z3	warm white	–
OptoSupply	OSPW5111B-QR	white	–
Toshiba	TLRE20TP	red	644
–	–	red	–
Marktech	MTE6800N2-UR	Infrared (IR)	680
Marktech	MTE1074N1-R	IR	740
Marktech	MTE1077N1-R	IR	770
–	IR-810	IR	810
Vishay	TSHG-8200	IR	830
OSRAM	SFH 4550	IR	850
OSRAM	SFH 4555	IR	850
OSRAM	SFH 4350	IR	860
Vishay	TSHA6200	IR	875
Vishay	TSHA6203	IR	875
–	IR-870	IR	870
OSRAM	SFH 483	IR	880
OSRAM	SFH 485	IR	880
Vishay	TSHF5210	IR	890
Toshiba	TLN110	IR	940
Kodenshi Corp.	EL-1CL3	IR	940
OSRAM	SFH 4545	IR	950
Omron	–	IR	660 and 955

# Appendix B

## Manual

In this chapter, a manual for reproducing the stated results is presented.

### B.1 Installation

First, the program has to be compiled since it is written in C++. The compilation pre-requisites are:

- `cmake`,
- `g++` with `c++11` support,
- `opencv`,
- `git`,
- `boost`,
- `libpointmatcher`
- `libsvm`

If this software is installed on your machine, follow next steps.

```
# cd src/VeinRecognition
# mkdir build && cd build
# cmake ..
# make
```

After that, the `VeinRecognition` evaluation application is successfully built on your system.

### B.2 Usage

For full documented usage run:

```
# ./VeinRecognition
```

For example, if you want to run an evaluation with a liveness detection mode for LBP features and use histogram comparison as a quality assessment method you simply run:

```
# ./VeinRecognition --liveness-detection --lbp --qa=histogram
```